DEPOSITIONAL PROCESSES AND ENVIRONMENTS IN WOLFCAMPIAN-LEONARDIAN STRATA, SOUTHERN MIDLAND BASIN, TEXAS

By

ZAKORY DEAN WARD

Bachelor of Science in Geology

Iowa State University

Ames, Iowa

2013

Submitted to the Faculty of the
Graduate College of the
Oklahoma State University
in partial fulfillment of
the requirements for
the Degree of
MASTER OF SCIENCE
May, 2017

DEPOSITIONAL PROCESSES AND

ENVIRONMENTS IN WOLFCAMPIAN-LEONARDIAN

STRATA, SOUTHERN MIDLAND BASIN, TEXAS

Thesis Approved:

Dr. Jack C. Pashin

Thesis Advisor

Dr. Jim Puckette

Dr. Mary Hileman

ACKNOWLEDGEMENTS

Foremost, I would like to thank my advisor, Dr. Jack Pashin, for his guidance, insight, and support throughout the course of this research. Additionally, thank you to my committee members, Dr. Jim Puckette and Dr. Mary Hileman, for their guidance and support over the last few years. I would like to give thanks to my colleagues and the department faculty and staff for making my time at Oklahoma State University a great experience. Special thanks to my family and friends for their continued support throughout my academic career. Finally, I would like to thank EOG Resources for their support. This study would not have been possible without support from EOG Resources, who funded this research and provided the core and associated data.

Name: ZAKORY DEAN WARD

Date of Degree: MAY, 2017

Title of Study: DEPOSITIONAL PROCESSES AND ENVIRONMENTS IN WOLFCAMPIAN-LEONARDIAN STRATA, SOUTHERN MIDLAND BASIN, TEXAS

Major Field: GEOLOGY

Abstract:

The Early Permian (Wolfcampian-Leonardian) Wolfcamp interval of the Permian Basin in West Texas is a mixed siliciclastic-carbonate succession that hosts one of the most important unconventional oil and gas plays in the world. Wolfcamp strata comprise stacked, cyclic gravity flow deposits separated by hemipelagic mudstone and siltstone. Interest in the geologic heterogeneity of these deposits and its effect on well performance has sparked research on the sedimentological, geophysical, and geochemical signatures and their correlation to depositional environments and reservoir properties.

This investigation analyzed a stratigraphic test core and associated laboratory data from the Wolfcamp play to help refine interpretations of the late Wolfcampian to early Leonardian succession in the southern Midland Basin. Detailed core descriptions and petrographic analyses were integrated with geochemical data to define facies, evaluate vertical stratigraphic successions, and relate reservoir properties with specific facies and depositional sequences. Interpretation of stratal stacking patterns and gravity flow transport processes were used to determine how vertical variations in rock fabric may be related to base level fluctuations and the morphology of platform margins and slopes. Sequence stratigraphic interpretations were made to help develop a predictive depositional framework.

Based on the characteristics and distribution of gravity flow deposits and interbedded hemipelagic sediment, a distal toe-of-slope to basin plain setting is inferred. In these settings, quartz and organic matter accumulated as background sedimentation interrupted by episodic deposition of gravity flows derived from the continental platform. Cyclicity is observed in individual, upward-fining trends of relatively coarse-grained skeletal material overlain by calcareous and/or siliceous mudstone. It is interpreted that the majority of gravity flows occurred during lowstands of relative sea level. Widespread pyrite and phosphatic nodules and TOC content as high as 8% indicates that low oxygen levels prevailed during accumulation of these sediments.

TABLE OF CONTENTS

Chapter Page

LIST OF TABLES

Table Page

LIST OF FIGURES

Figure Page

Figure Page

CHAPTER I

INTRODUCTION

The Wolfcamp is a major unconventional oil and gas play in the Permian Basin. Unconventional plays constitute laterally or vertically extensive oil and gas reservoirs characterized by low matrix permeability. The extensive distribution of these plays, which can extend through large parts of sedimentary basins, can significantly reduce development risks; small-scale geologic heterogeneities ultimately control reservoir quality and production performance (Spain and Anderson, 2010).

The commercial recovery of large volumes of oil and gas from unconventional reservoirs was made possible by a combination of precision directional drilling and multi-stage hydraulic fracturing. Innovations facilitating the modern application of this technology include measurement while drilling coupled with accurate and responsive gyroscopic geosteering. In 2004, lessons learned from experimentation with these technologies in the Barnett Shale of north-central Texas were applied to the Permian Basin, breathing new life into one of the oldest and most prolific sedimentary basins in the U.S. Since 2007, the advent of shale oil development has reversed declining production and declining rig count (Kelley et al., 2012). Indeed, operators have discovered that many of the zones that were historically bypassed, like the Wolfcamp, have major economic potential.

The shift in industry focus from conventional to unconventional reservoirs has led to a similar shift in academic research. Pre-1980's research in the Permian Basin was primarily focused on stratigraphic correlations, depositional processes, and geophysical characteristics of shallow platform and slope carbonate deposits. Recent interest in Late Paleozoic strata has led to new studies examining fine-grained siliciclastic and resedimented carbonate successions deposited basinward of the carbonate platforms. A wide range of depositional environments and flow processes in a lower slope to basinal setting resulted in irregularly mixed lithologies and complex structural relationships. The resulting depositional heterogeneity makes the distribution and quality of source rock and reservoir facies difficult to predict and has thus complicated oil and gas exploration in this region for decades. An improved understanding of depositional processes and environments that were active during Wolfcampian-Leonardian (Asselian-Kungurian) deposition is a critical component of characterizing Wolfcamp petroleum systems.

GOALS AND OBJECTIVES

The objective of this research is to characterize the nature of Wolfcampian-Leonardian deposition in the southern Midland Basin to improve understanding of the geologic heterogeneity responsible for variable reservoir quality and performance. The project incorporates well-established regional interpretations of depositional environments and stratigraphy with observations made on a representative core, and core data, from the active Wolfcamp play area in the southern Midland Basin (Figure 1). The core (Mayer 4901) covers a continuous stratigraphic section from upper Wolfcamp strata of the late Wolfcampian Series to the Dean Formation of the early Leonardian Series (Figure 2).

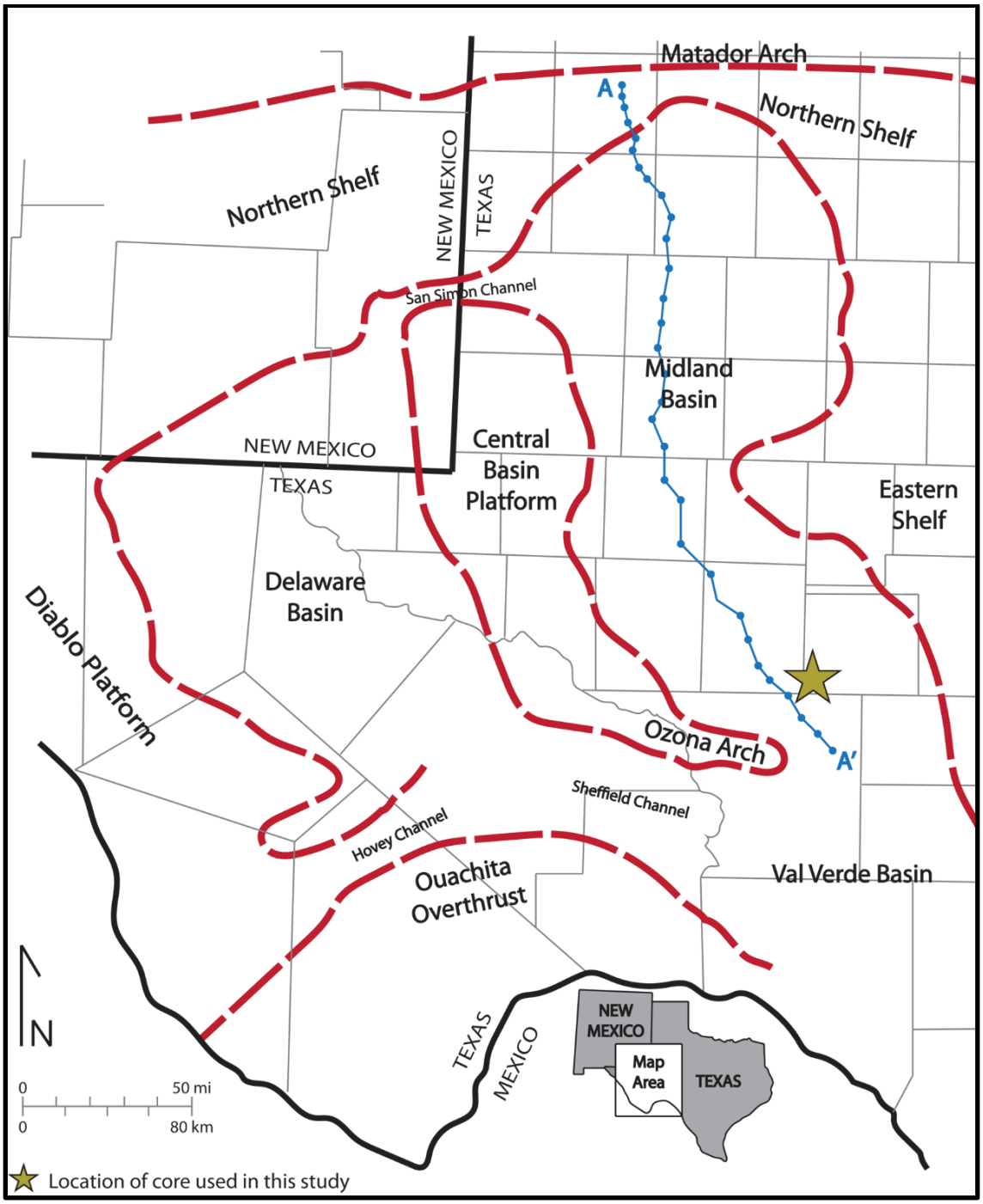

Figure 1. Major structural elements of the Permian Basin during Permian time showing location of a regional cross section and the core used in this study (modified from Ruppel, 2009).

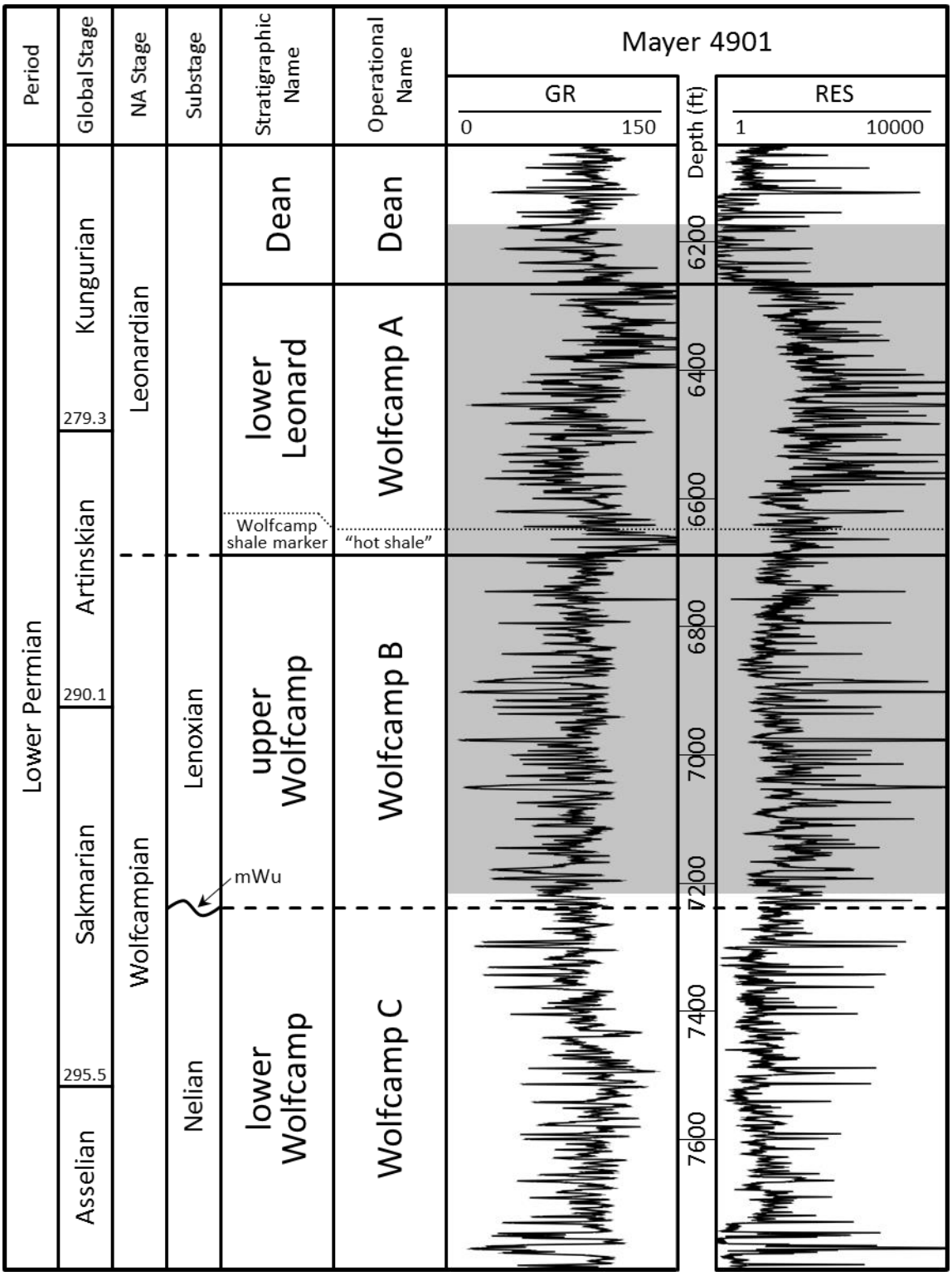

Figure 2. Stratigraphic and operational names of Wolfcampian and Leonardian strata in the Midland Basin area. Mayer 4901 well is in southwest Irion County, Texas. See figure 1 for location. Operational names are from Pioneer Natural Resources, 2013. Radiometric ages (in Ma) are from Henderson et al., 2012. Shaded area represents the cored interval. NA = North American; mWu = mid-Wolfcampian unconformity.

The Mayer 4901 core comprises a succession of various gravity flow deposits and interbedded hemipelagic sediment. Detailed core descriptions were used to define lithofacies, examine facies relationships, and relate reservoir attributes to interpreted depositional conditions. Basic principles of sequence stratigraphy and facies stacking patterns were evaluated to determine their spatial and temporal relationship to Wolfcampian-Leonardian platform successions.

The key questions to be addressed by this research are:

1. What was the environmental setting during deposition of Wolfcamp sediment?
2. What depositional processes were effective during Wolfcamp sedimentation, and at what rates did they operate?
3. How do depositional facies and vertical stratigraphic successions relate to paleoclimate, tectonics, and fluctuations of relative sea level?
4. Do facies and facies stacking patterns conform to regional sequence interpretations established by previous studies?

CHAPTER II

GEOLOGIC BACKGROUND

STRUCTURE AND TECTONICS

The study area is located near the paleogeographic center of the southern Midland Basin (Figure 1). The Midland Basin is one of several component basins of the greater Permian Basin that formed along the southern margin of the North American craton during Pennsylvanian-Permian time (Hills, 1984; Cys and Gibson, 1988; Ewing, 1993). The basin is bounded by tectonic uplifts and carbonate platforms including the Central Basin Platform on the west, the Ozona Arch on the south, and the Northern and Eastern Shelves (Figure 1).

Development of the Permian Basin can be divided into three stages. First, from Cambrian to Mississippian time, the Permian Basin region was part of a large cratonic basin called the Tobosa Basin (Hills, 1972). Sedimentation occurred mainly in shelf carbonate ramp environments (Hills, 1984). The second stage of tectonic evolution takes place from the Early Pennsylvanian to the Early Permian. During this time, the eastern North American craton collided with the South American craton, causing crustal flexure in the foreland of the Ouachita-Marathon orogenic belt. This flexure transformed the Tobosa Basin into a series of rapidly subsiding sub-basins separated by structural uplifts (Hills, 1984; Horak, 1985; Hills, 1972). By Late Pennsylvanian time, broad carbonate shelves had developed along the basin margins. Multiple pulses of tectonic activity,

coupled with glacial eustasy, generated complex platform to basin depositional sequences of alternating siliciclastic and carbonate strata (Silver & Todd, 1969; Veevers & Powell, 1987). The third stage of development, spanning Middle to Late Permian time, was a time of relative tectonic stability. Although sedimentary infilling continued, the rate of subsidence in the basins decreased substantially. Clastic sediment supply was reduced and carbonate shelves became more distinct reef-rimmed platforms.

By Wolfcampian-Leonardian time, uplift of the Central Basin Platform had divided the Tobosa Basin into two asymmetric northwest-elongate basins (Delaware, Midland) (Figure 1). In the Midland Basin, estimates of maximum water depth range from 1,000 ft. in the early Wolfcampian (Hobson et al., 1985) to 2,000 ft. in the early Leonardian (Montgomery, 1996). Photic zones around the basins lead to the growth of massive carbonate banks (Hills, 1984). At the same time thick sections of organic-rich Wolfcamp shale deposition accumulated in the deeper parts of the basins (Adams, 1965; Hills, 1972; Flamm, 2008). Regionally, the Wolfcamp thickens to the southeast, where a gap between the Ozona Arch and the Eastern Shelf connects the Midland Basin to the Val Verde Basin (Figure 1) (Hamlin and Baumgardner, 2012).

REGIONAL STRATIGRAPHY AND SEDIMENTATION

Chronostratigraphic and lithostratigraphic nomenclature of Wolfcamp and Leonard strata in the Midland Basin is shown in Figure 2. Microfossil dating and correlation in the last few decades has resulted in redefinition of the top and base of the Wolfcampian Series. The most recent definition has resulted in an upward shift of the base of the Wolfcampian Series, reassigning rocks that were previously thought to be the earliest Wolfcampian, sometimes called the Cline Shale, to the Virgilian Series (Late Pennsylvanian). The top of the Wolfcampian Series in the Midland Basin now occurs in

what is commonly referred to as the “Wolfcamp shale marker,” therefore reassigning rocks that were previously thought to be the latest Wolfcampian to the lower Leonardian (Hamlin and Baumgardner, 2012). This study uses nomenclature consistent with the stratigraphic classification and log-based correlations for the Wolfcamp-lower Leonard interval published by Hamlin and Baumgardner (2012) (Figure 2).

The Wolfcamp is largely a two-rock-type system dominated by shale interbedded with limestone (e.g. Wilson, 1975; Mazzullo and Reid, 1989; Walker et al., 1991; Hamlin and Baumgardner, 2012). Hamlin and Baumgardner (2012) performed a core-based geochemical study of the basinal Pennsylvanian-Permian section of the southern Midland Basin (Figure 3). Elemental data were collected and used to define facies and describe chemostratigraphic variation. Four facies were observed: 1) siliceous mudrock, 2) calcareous mudrock, 3) muddy carbonate-clast conglomerate, and 4) skeletal packstone/grainstone. The first two facies were interpreted as hemipelagic deposits. The second two were interpreted as mostly sediment gravity-flow deposits based on poor sorting and graded bedding seen in core (Hamlin and Baumgardner, 2012).

Proximal to the Central Basin Platform and Northern and Eastern shelves, the Wolfcamp is composed of a variety of resedimented carbonate deposits, including breccia, skeletal sand, and lime mud deposited by a spectrum of sediment gravity flow processes (e.g., slumps, debris flows, grain flows, and turbidity currents) and bottom currents on the lower slope and basin floor (Hobson et al., 1985; Mazzullo and Reid, 1987; Mazzullo and Reid, 1989). Hobson and others (1985) examined roughly 600 thin sections in the southern Midland Basin to establish a biostratrigraphic framework for

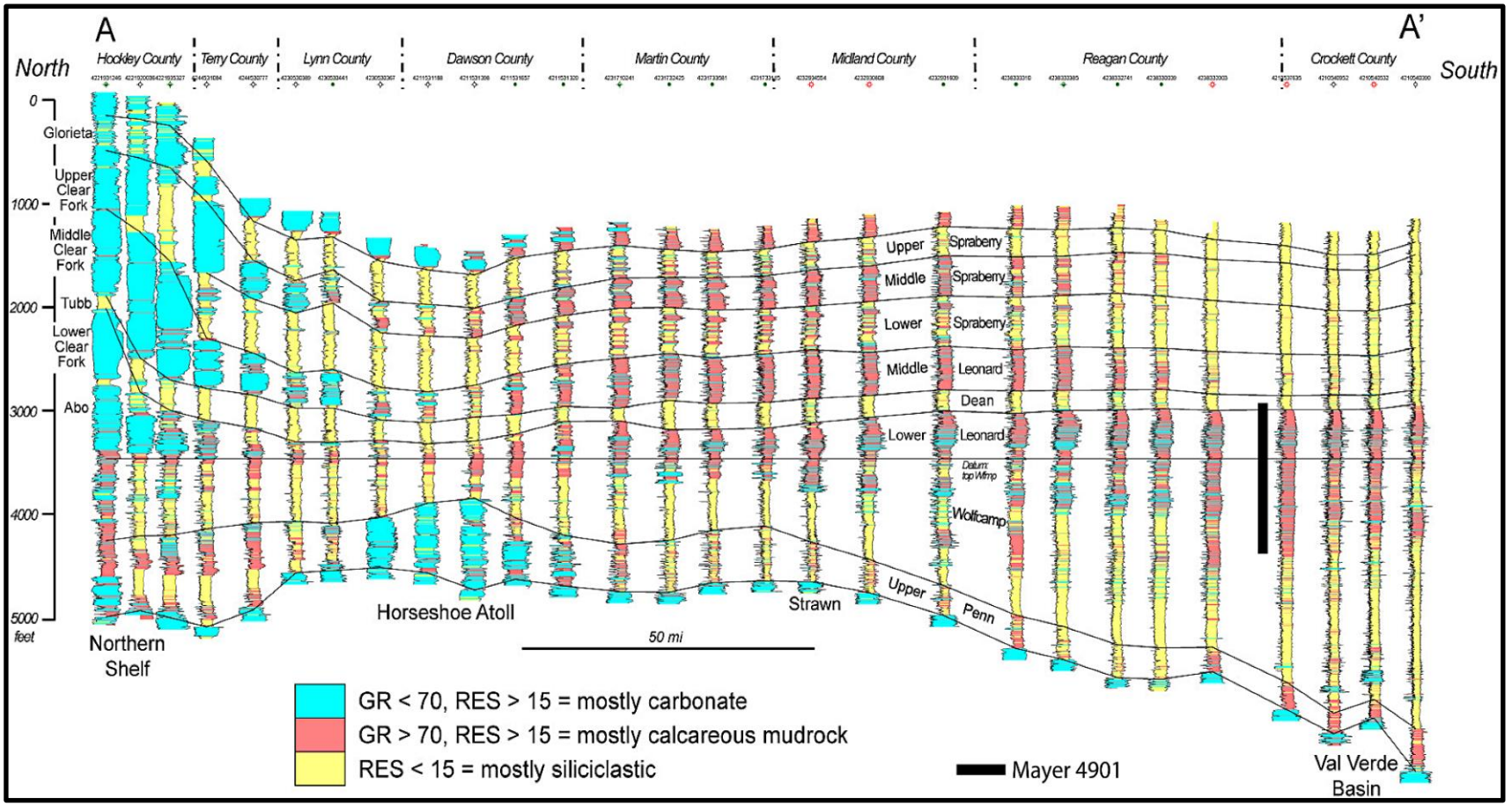

Figure 3. Cross section A-A' from Figure 1 showing basic facies relationships in the Midland Basin and relative location of the cored interval used in this study. Modified from Hamlin and Baumgardner, 2012.

early Wolfcamp carbonate deposits. Thin shale breaks, changes in matrix composition, and vertical variation in lithoclast lithology suggest that sedimentation was episodic.

The Carboniferous-Permian was a time of continental glaciation in Gondwana (Veevers and Powell, 1987; Fielding et al., 2008). Glaciation drove high amplitude (tens of meters) and high frequency (~41 kyr) eustatic sea level changes (Heckel, 1986; Saller et al., 1994; Fielding et al., 2008). The flooding and exposure of the wide platforms due to sea-level fluctuation controlled sediment input (Heckel, 1986). During sea-level lowstands, platforms were exposed and sediment was transported directly into the basin by gravity flow processes. During sea-level highstands, flooded platforms became carbonate factories, and sediment transported into the basin was composed of platform-derived carbonate material and hemipelagic, windblown silt and clay. The hemipelagic part of the system was active throughout the sea-level cycles, because organic matter and siliciclastic silt are abundant in all basinal intervals (Hamlin and Baumgardner, 2012).

CHAPTER III

METHODS

This study focused on a single core (Mayer 4901) from Irion County, Texas (Figure 1). EOG Resources drilled the well for salt water disposal and recovered the core to evaluate Wolfcamp reservoir properties. Core and lab data were prepared by Core Laboratories, Inc. and donated to this study by EOG Resources. The core is of H-gauge (3.5-in. diameter) and spans measured depths from 6,163 ft. to 7,212 ft., thus covering 1,049 ft. of strata assignable to the Wolfcamp and Dean formations. In this study, the core was used to (1) define lithofacies, (2) interpret depositional processes and environments, (3) evaluate lithologic order, (4) identify key stratigraphic surfaces and define depositional sequences and parasequences, and (5) relate the stratigraphic and depositional framework to sequence interpretations established by earlier studies.

Observations were made using slabbed core and core photos taken in white and ultraviolet light. The core was described at a centimeter resolution to define rock type, color, texture, bedding, physical sedimentary structures, and biogenic sedimentary structures. The degree of bioturbation (BI) was indexed on a scale of 0-6 (0=absent, 6=homogenized) following Bann et al. (2008). Stratigraphic columns were generated using Adobe Illustrator. Observations were systematically recorded in a stratigraphic table designed in Adobe Illustrator followed by a statistical summary in an Excel spreadsheet.

Lithofacies were then defined using guidelines proposed by Lazar and others (2015), and a preliminary interpretation of depositional process and environment was made based on comparison with the available literature. The arrangement of rock types and lithofacies was used to define larger lithologic packages based on their stacking patterns (i.e., aggradational, retrogradational, and progradational). Where necessary, the core was sprayed with water to help reveal lithologic detail. Ten percent HCl solution was applied to the exterior of the core where necessary to identify limestone and other calcareous materials.

Stratigraphic columns were constructed to facilitate evaluation of trends of grain size and bed thickness, as well as vertical trends of lithofacies and sediment stacking. Key stratigraphic surfaces and intervals were identified based on the results of this analysis and include condensed sections, parasequences, and depositional sequences. Results of this analysis were then visually compared to the relative sea level curve for the Midland Basin proposed by Mazzullo and Reid (1989), to test for conformance with previous interpretation. Regional Wolfcampian-Leonardian sequence interpretations established by earlier studies were used to support depositional interpretations in this study.

Thin sections and thin section photomicrographs were prepared by Core Laboratories, Inc. from samples collected at ~10-ft. intervals throughout the core. These samples were used to augment visual observations of slabbed core. The thin sections were used to classify the rocks using the modified Dunham classification of Embry and Klovan (1971). The thin sections also helped define vertical and lateral heterogeneity at the microscopic scale and were used to identify microscale sedimentary, biological, and diagenetic features. Thin sections were impregnated with blue epoxy to reveal porosity and stained with alizarin-red for identification of calcite and dolomite.

X-ray diffraction (XRD) analysis was performed by Core Laboratories, Inc. Samples for XRD were taken from the same depth as the thin sections to provide a qualitative and semi-quantitative determination of whole rock mineralogy. These data were integrated with the core description and thin section analyses to aid in lithologic characterization. These data also helped inform interpretations of depositional processes and environments.

Petrophysical data from the Mayer 4901 well was measured and prepared by Core Laboratories, Inc. These data include: sample depth, porosity, permeability, bulk density, and TOC and fluid saturation (i.e. water, oil, and gas). These data were analyzed to compare and identify associations of reservoir properties and particular facies.

CHAPTER IV

LITHOFACIES AND DEPOSITIONAL PROCESSES

LITHOFACIES ANALYSIS

The upper Wolfcamp-Dean succession comprises variety of resedimented carbonates and siliciclastics, most of which are dominated by fine-grained (clay- to silt-size) sediment. For the purposes of this study, six lithofacies have been defined: 1) packstone-grainstone, 2) floatstone-rudstone, 3) wackestone-packstone, 4) silty sandstone, 5) muddy siltstone, and 6) siliceous to calcareous mudstone (Table 1, Figure 4). A fundamental understanding of the mechanics of subaqueous sediment transport and deposition is based on the internal characteristics of these deposits. Following a description of each lithofacies, interpretations of associated depositional processes are made.

LITHOFACIES 1. PACKSTONE-GRAINSTONE

CHARACTERISTICS

The packstone-grainstone lithofacies is composed mostly of silt to coarse sand-size skeletal carbonate grains in a light gray to gray crystalline cement of calcite or dolomite. Individual beds are mostly massive, but many feature normal or inverse grading (Figure 5). Bed thickness ranges from 3 to 24 in. thick. Diffuse planar laminae

Lithofacies		Color	Mineralogy (Avg. %)				Sedimentological Character	Composition	TOC (Avg. %)	Porosity (Avg. %)	Perm. (Avg. mD)
			Carbonate	Clay	Q+F	Other					
1	Packstone-Grainstone	Light Gray to Gray	67	5	22	6	Massive to inversely graded, grain-dominated, sharp bedding contacts	Silt- to coarse sand-size carbonate grains, minor quartz silt	0.32	3.10	0.229
2	Floatstone-Rudstone	Light Gray to Dark Grayish Brown	X	X	X	X	Sand to pebble-size clasts in fine-grained matrix, clast to mud-dominated, chaotic texture, bioclastic dikes, sharp bedding contacts	Matrix: carbonate mud Clasts: carbonate lithoclasts and bioclasts	X	X	X
3	Wackestone-Packstone	Light Gray to Gray	53	15	24	8	Normally graded, planar and cross-laminae, erosional basal contacts, partial Bouma sequences	Silt- to sand-size carbonate grains; argillaceous carbonate mud matrix; minor quartz silt, clay, and organic matter	1.97	5.47	0.157
4	Silty Sandstone	Light Gray to Grayish Brown	10	8	76	6	Massive to normally graded, planar and cross-laminae, erosional basal contacts, partial Bouma sequences	Fine- to very fine sand, coarse silt, dolomite cement, minor clay	0.34	4.91	0.102
5	Muddy Siltstone	Light Brownish Gray to Very Dark Grayish Brown	8	27	57	8	Planar-parallel laminated to intensely and diversely bioturbated, alternating silt/mud composition	Silt, clay, and organic matter	2.36	8.91	0.240
6	Siliceous Mudstone	Dark Gray to Very Dark Gray	12	33	45	10	Massive to weakly laminated, phosphatic nodules, locally bioturbated	Argillaceous mud, quartz silt, and organic matter	3.93	9.12	0.150
	Calcareous Mudstone	Gray to Dark Gray	49	13	27	11	Massive to weakly laminated, locally bioturbated	Carbonate mud and silt, organic matter, quartz silt	2.81	7.37	0.055

Table 2. Lithofacies summary and diagnostic attributes. Bioturbation

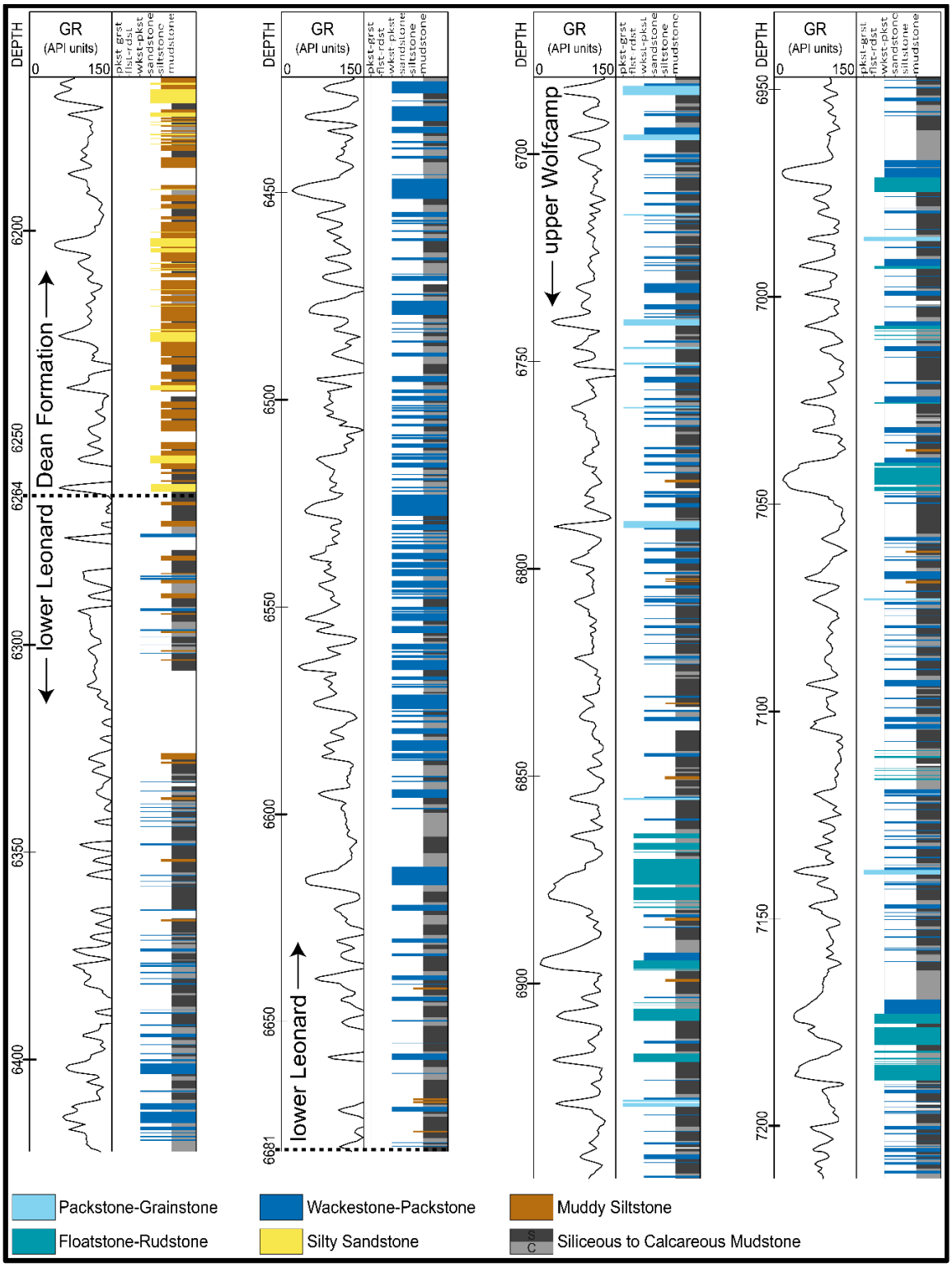

Figure 4. Lithofacies interpreted from Mayer 4901 core. The upper Wolfcamp is dominated by siliceous mudstone with intercalated carbonate-rich facies. Abundance of wackestone-packstone and calcareous mudstone increases in the lower Leonard. The Dean Formation is comprised of primarily muddy siltstone and silty sandstone. GR = gamma ray.

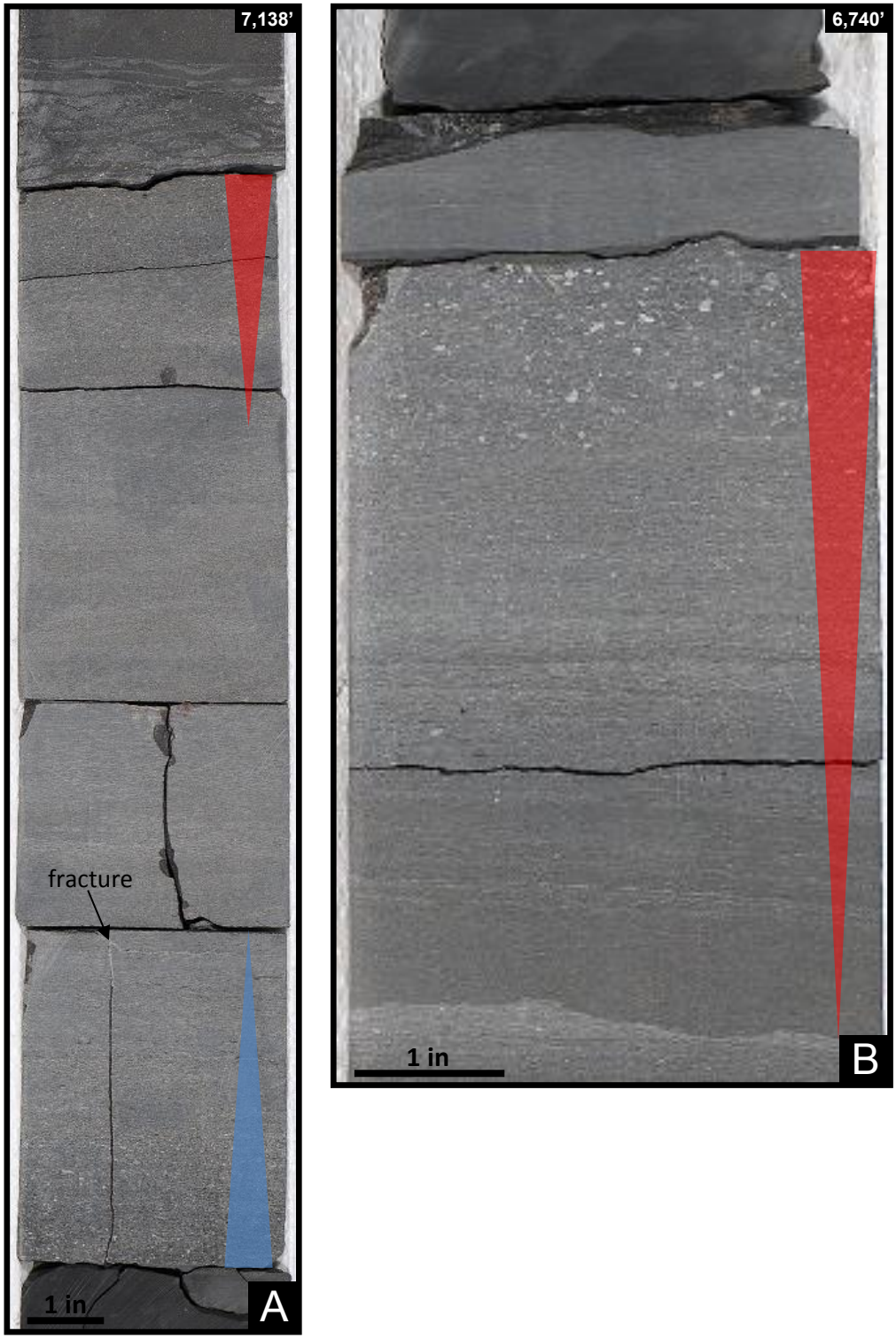

Figure 5. Core photographs of packstone-grainstone. A) Packstone-grainstone bed displaying normally graded base and inversely graded top. Chaotically mixed, finer-grained sediments directly overlying the top indicates turbulence, possibly generated by shear mixing at the upper interface of the grainflow. Mineralized fractures are identified in the lower portion of the bed. B) Inversely graded bed showing diffuse planar laminae and sharp upper and lower contacts.

distinguished by slight variations in color and texture are observed in some beds (Figure 5B). Lower and upper contacts are typically sharp (Figure 5), although upper contacts may be gradational with the wackestone-packstone lithofacies. Calcite-filled fractures occur locally (Figure 5A). Packstone-grainstone is interspersed throughout the upper Wolfcamp section only (Figure 4, Appendix).

Thin sections and XRD data show that this facies consists predominantly of calcite (avg. 62%) and quartz (avg. 19%). Alizarin red stain reveals that calcite occurs as skeletal grains, cement, and micritic matrix (Figure 6). Partial dissolution and dolomitization of skeletal grains is common. Skeletal material is mostly fragmented and consists of crinoids, brachiopods, bryozoans, phylloid algae, sponge spicules, fusulinids, and other foraminifera (Figure 6). Thin section examination also shows that minor amounts of clay- and organic-rich particles are scattered throughout the skeletal framework of some beds (Figure 6). Average TOC in this facies is 0.32%.

DEPOSITIONAL PROCESSES

Based on common inverse grading and sharp upper and lower contacts, packstone-grainstone lithofacies are interpreted as grain flow deposits or the bedload layer of some high-density turbidity current deposits. Grain flows are liquefied, cohesionless flows in which the intergranular friction between grains is reduced by grain-to-grain interactions (Selley, 2000). Particle collisions generate a dispersive pressure that helps prevent grains from settling out of suspension, thereby resulting in laminar flow (Lowe, 2006; Talling et al., 2012).

Many of the bioclasts identified (brachiopods, phylloid algae, and fusulinids) were inhabitants of shelf environments while living (Scholle and Ulmer-Scholle, 2003) indicating that grain flows originated on shallow-water shelves or their margins. Pure

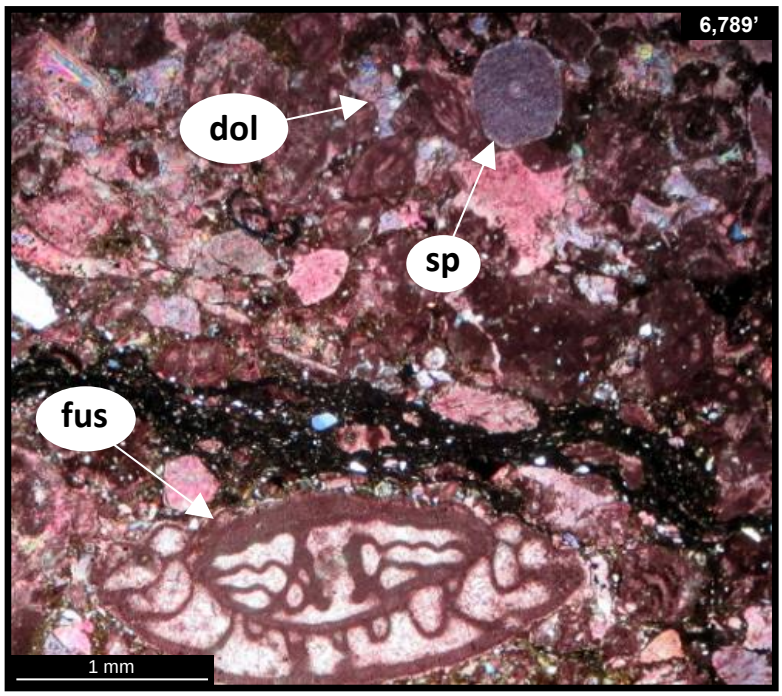

Figure 6. Thin section photomicrograph of packstone-grainstone facies in cross-polarized light. A clay- and organic-rich layer is compacted into the skeletal framework. Calcite is present as matrix material, cement, and skeletal grains such as fusulinids (fus) and sponge spicules (sp). Dolomitization and dolomite (dol) cement is also observed.

grain flows require high slope gradients for initiation and a confined space to retain the high pore pressure required for continued flow. However, modification by inclusion of small amounts of clay can significantly elevate pore-fluid pressures, permitting flow on gentle slopes (Selley, 2000; Lowe, 2006; Pickering and Hiscott, 2016). Cohesion supported by a small amount of interstitial mud leads to increased traction efficiency facilitating the development of laminae in modified grain flows (Low et al., 2003). Small amounts of clay identified in thin section and planar laminated traction structures observed in core indicate that grain flows interpreted in Mayer 4901 are likely to have occurred as modified grain flows and not true grain flows.

As evidenced by inverse grading and sharp upper contacts, packstone-grainstone deposits represent flows with higher sediment concentrations and densities

than the normally graded beds typically associated with turbidity currents. However, intense grain interaction at the base of high-density turbidity currents, as well as debris flows, may also produce traction structures and other features reminiscent of grain flows.

LITHOFACIES 2. FLOATSTONE-RUDSTONE

CHARACTERISTICS

The floatstone-rudstone lithofacies comprises mixtures of matrix- and clast-supported bio- and lithoclasts. Matrix material is mud-rich, calcareous, and gray to dark grayish brown. Clasts are irregularly distributed and primarily coarse sand to pebble-size. Lithoclasts are mostly subangular to subrounded bioclastic packstone and grainstone. Bioclasts are primarily disarticulated and fragmented. Large variations in bedding attitude along with chaotic bedding and bioclastic dikes are the defining features (Figure 7). Contorted bedding and irregular ptygmatic folds are observed in some finer-grained intervals (Figure 8B). Lower and upper contacts are commonly sharp. Floatstone-rudstone beds range in thickness from 1 to 7 ft. and are identified only in the upper Wolfcamp interval below 6,864 ft. (Figure 4, Appendix).

Floatstone-rudstone generally display poorly sorted textures (Figure 8A); however, normal and inverse grading produced by traction is observed within some grain-supported intervals. Sedimentary structures such as laminae and scour surfaces are preserved locally. Microfaults are common within this lithofacies (Figure 7). Flattened and internally deformed mud clasts ranging from pebble to cobble size are generally concentrated near the base or in the middle of the beds (Figure 7). Bioclasts identified in core include crinoids, corals, brachiopods, bryozoans, phylloid algae, and fusulinids.

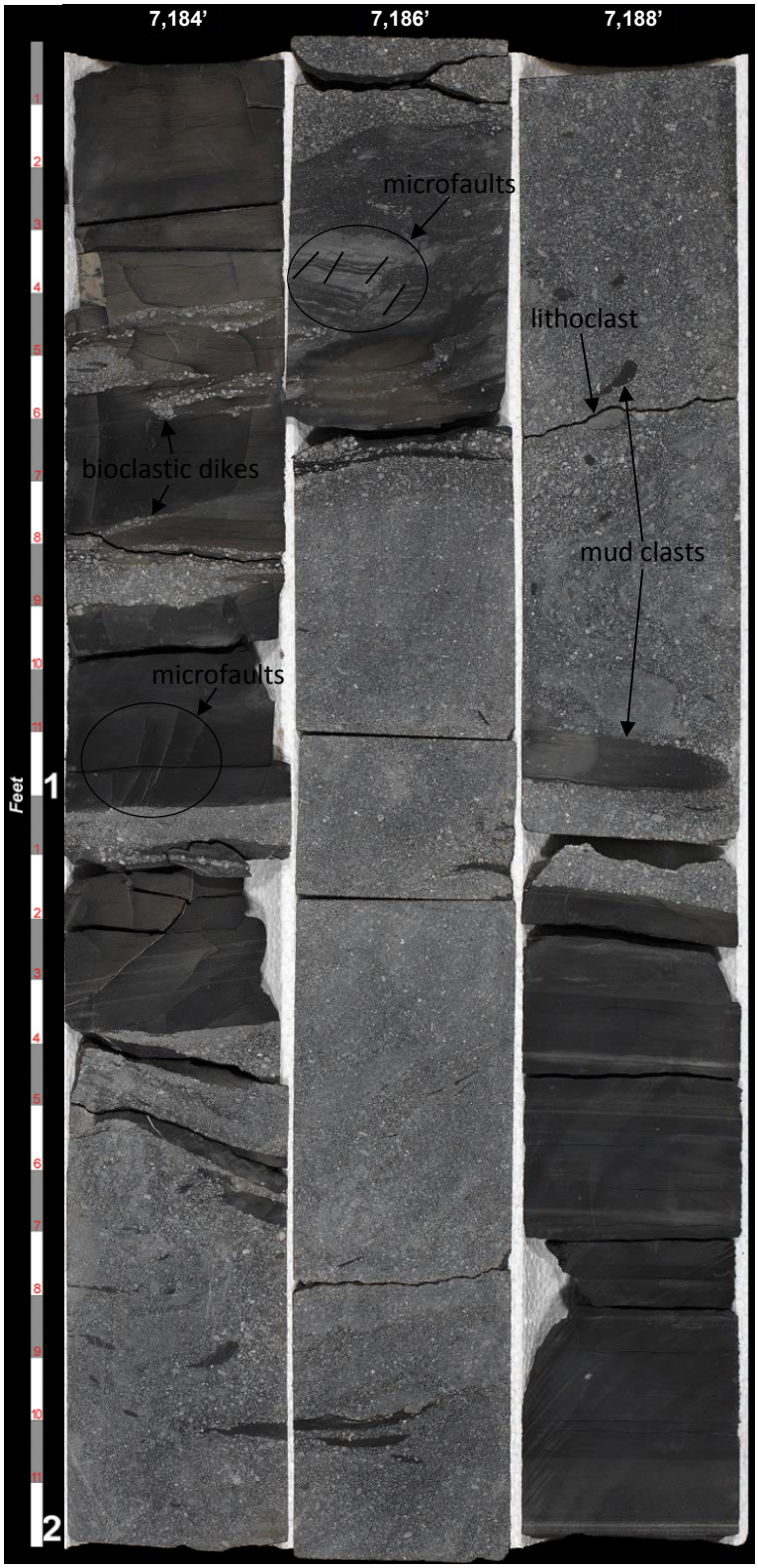

Figure 7. Core photograph of floatstone-rudstone showing rotated and contorted bedding, randomly oriented mud clasts, and poorly sorted carbonate clastic material. Thin, clastic-rich layers (bioclastic dikes) appear to have been forcefully injected into mud-rich intervals during flow. Microfaults and pyrite are also observed.

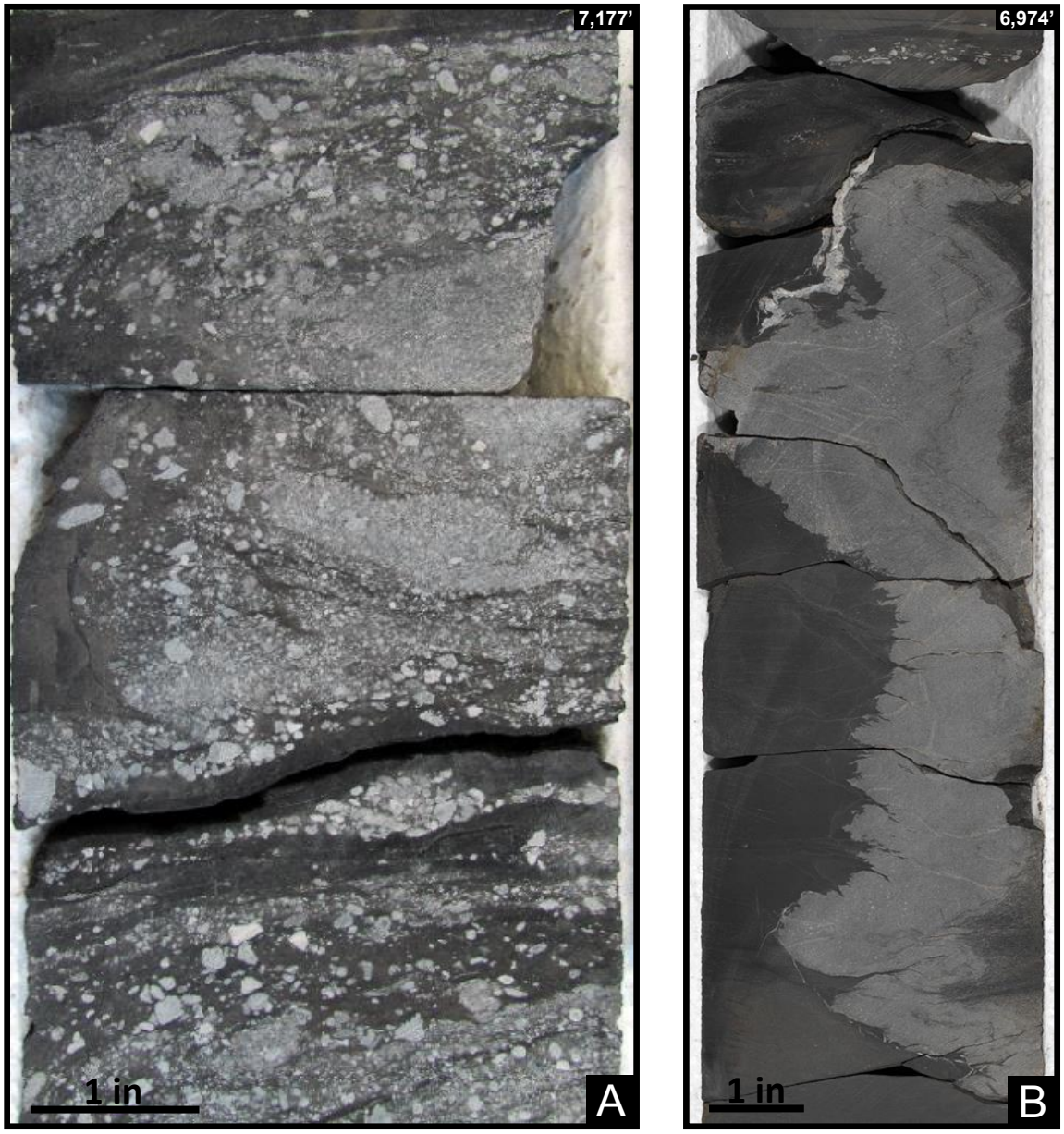

Figure 8. Core photographs of floatstone-rudstone. A) Floatstone showing chaotic distribution of coarse sand to pebble-size bioclasts and lithoclasts. B) Ptygmatic folding of fine-grained carbonate material.

DEPOSITIONAL PROCESSES

Based on mixing of matrix- and grain-supported textures, chaotically distributed clasts, and lack of vertical grading and sedimentary structures, floatstone-rudstone are interpreted as debris flow deposits. Debris flows, also known as debrites, consist of

cohesive mixtures of granular solids, clay minerals, and water that behave plastically under high strain. Particle support and buoyancy during flow comes from a combination of forces including frictional resistance to settling, cohesion between clay-size particles, and elevated pore pressures. (Mulder and Alexander, 2001; Posamentier and Martinsen, 2011; Pickering and Hiscott, 2016). When the critical yield strength of the flow falls below the gravity imposed shear stress the flow freezes *en masse* (Talling et al., 2012).

As with packstone-grainstone, many of the bioclasts identified (corals, brachiopods, phylloid algae, and fusulinids) lived in shallow-water settings indicating that floatstone-rudstone were transported from adjacent shelf areas. Injection of bioclastic material into muddy layers is common and likely the result of sediment loading and dewatering. Zones with contorted bedding and imbricated clasts may have resulted as a consequence of shearing. Though commonly associated with a lower slope setting, debris flows can travel across extremely low-gradient slopes and have been found to extend onto the basin floor 60 miles from their source (Crevello and Schlager, 1980; Shanmugam, 2012).

LITHOFACIES 3. WACKESTONE-PACKSTONE

CHARACTERISTICS

The wackestone-packstone lithofacies is abundant throughout most of the upper Wolfcamp and lower Leonard intervals (Figure 4, Appendix). These deposits are dominantly skeletal and tend to be argillaceous. Individual beds range in thickness from less than 1 to 60 in., but most are less than 6 in. Wackestone-packstone are light gray to gray in color and structureless or normally graded and/or laminated. Scattered carbonate skeletal debris in a clay- and silt-rich matrix often giving this facies a faint salt-and-

pepper appearance (Figure 9A). Much of the skeletal material is macerated, but whole specimens of brachiopods, crinoid stems, and fusulinids are present locally.

Lower contacts are sharp and often display sole marks. Packstone layers generally occur in the basal portions of normally graded beds and typically contain planar laminae or are structureless (Figure 9A and 10). Wackestone also may be structureless or laminated. A typical succession fines upward from skeletal-rich packstone to skeletal wackestone to calcareous and/or siliceous mudstone. In the lower Leonard, these successions are locally stacked (Figure 9A). Current structures are common in beds thicker than 6 in., including low angle cross-strata, vergent flame structures, ripple cross-laminae, and internal erosional contacts (Figures 9B and 10). Soft-sediment deformation structures such as convoluted bedding, loop bedding, and flame structures are locally common (Figures 9B, 10, and 11A). Chert bands or lenses, distinguished by a dark bluish gray color, occur locally and are often rimmed by pyrite (Figure 11B). Although rare, burrows were identified in some wackestone layers (Figure 9A).

Combined XRD and thin section analyses show this facies consists primarily of calcite (avg. 48%), quartz (avg. 20%), and clay (avg. 15%). Alizarin red stain reveals calcite is present as skeletal grains, cement, and matrix material (Figure 12). Quartz occurs as detrital silt. Microfossils, such as benthic foraminifera and sponge spicules, are common and abundant in most samples (Figure 12). In some samples, concentrated skeletal fragments define laminae. XRD data show that clay is mostly illite-mica. Pyrite (avg. 3%) commonly occurs as clusters of crystals in bioclasts and along bedding planes (Figure 12). Average TOC in this facies is 1.97%.

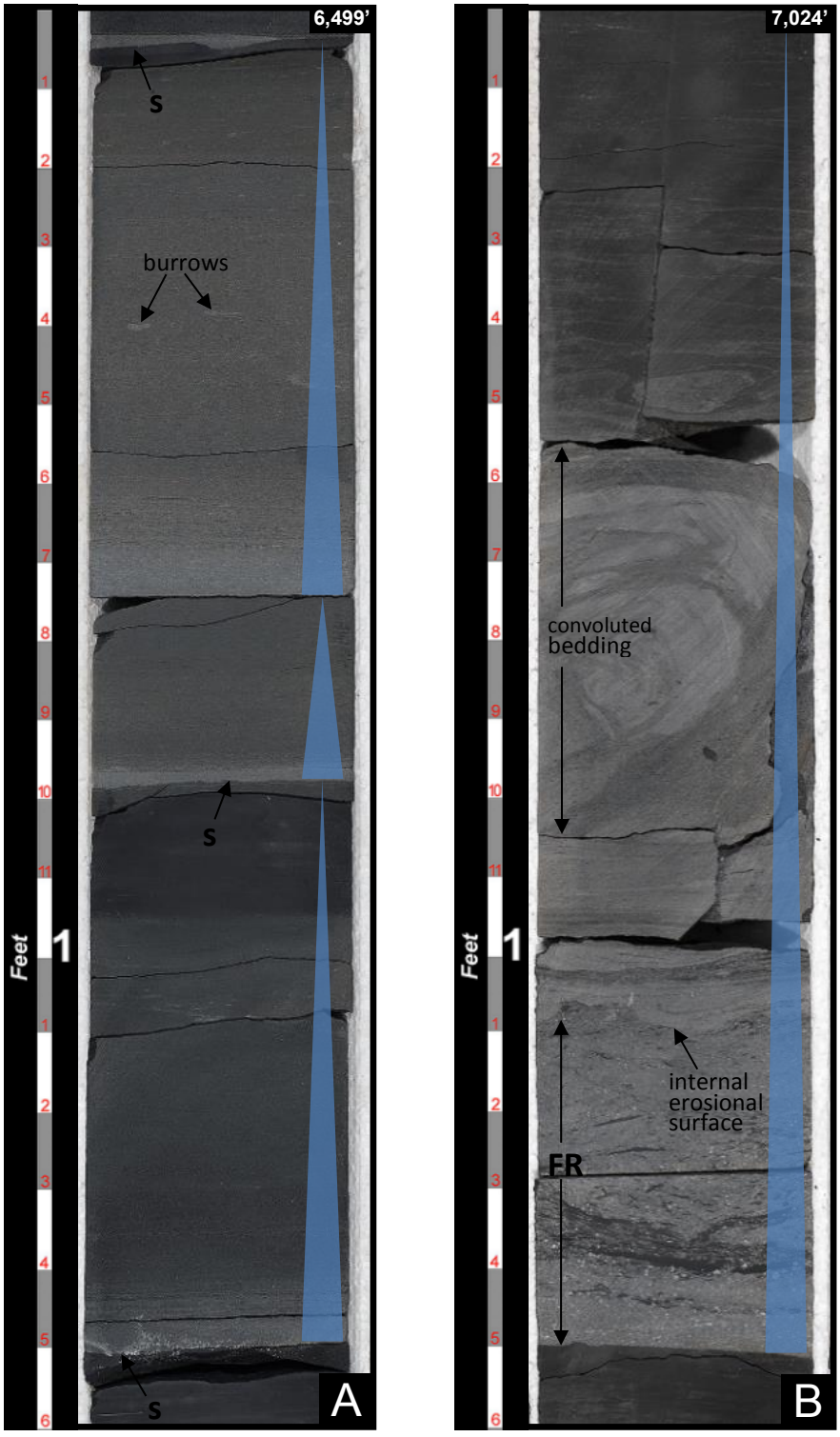

Figure 9. Core photographs of wackestone-packstone. A) Stacked, normally graded wackestone-packstone beds showing fining upward succession from packstone to wackestone and/or mudstone. Sole marks (s), unidentified burrows are observed in the uppermost bed. B) An internal erosional surface defines the boundary between normally graded and convoluted wackestone-packstone (top) and unsorted floatstone-rudstone (bottom).

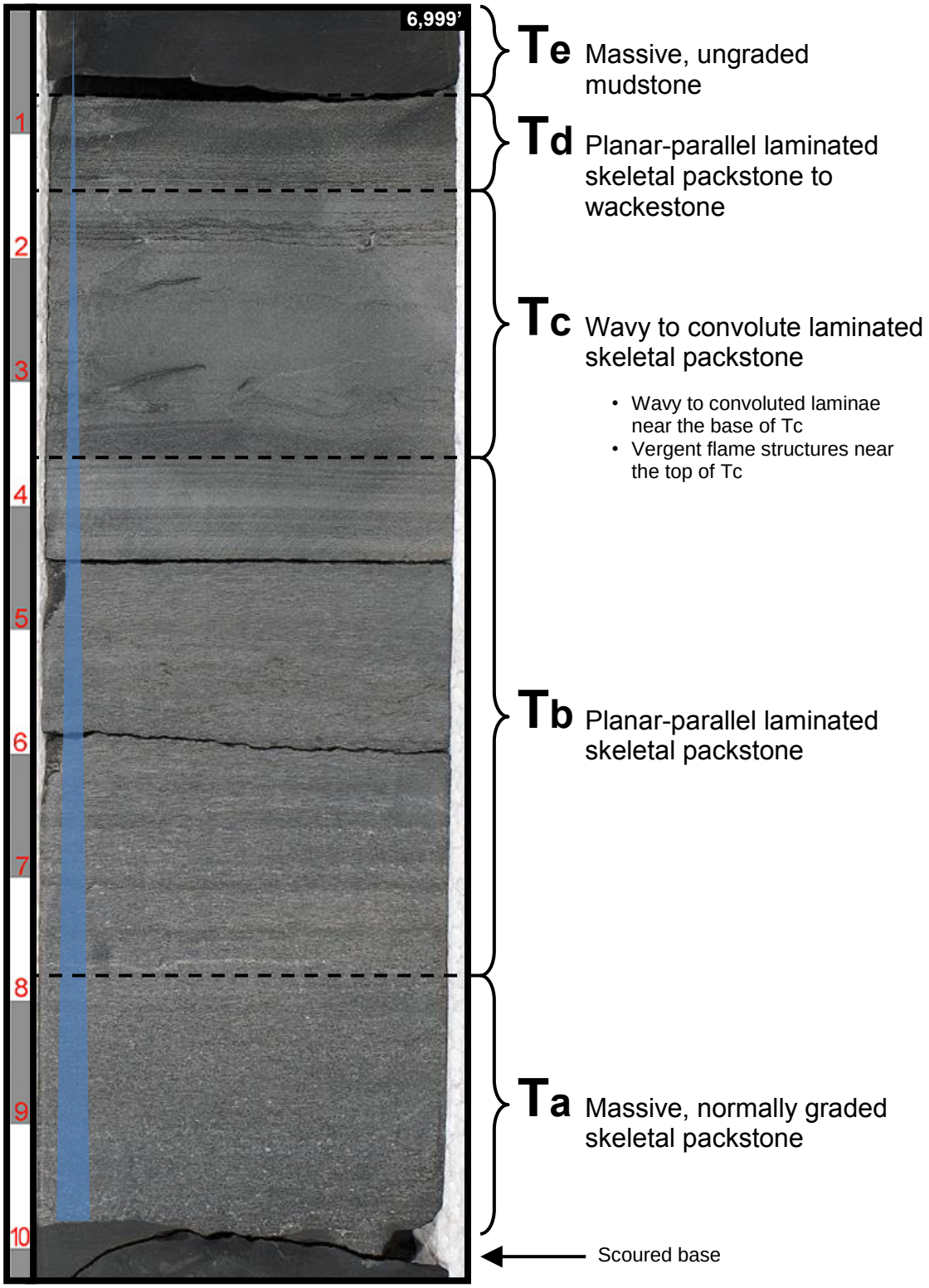

Figure 10. Core photograph of wackestone-packstone showing grading and internal structures consistent with Bouma divisions Ta-e.

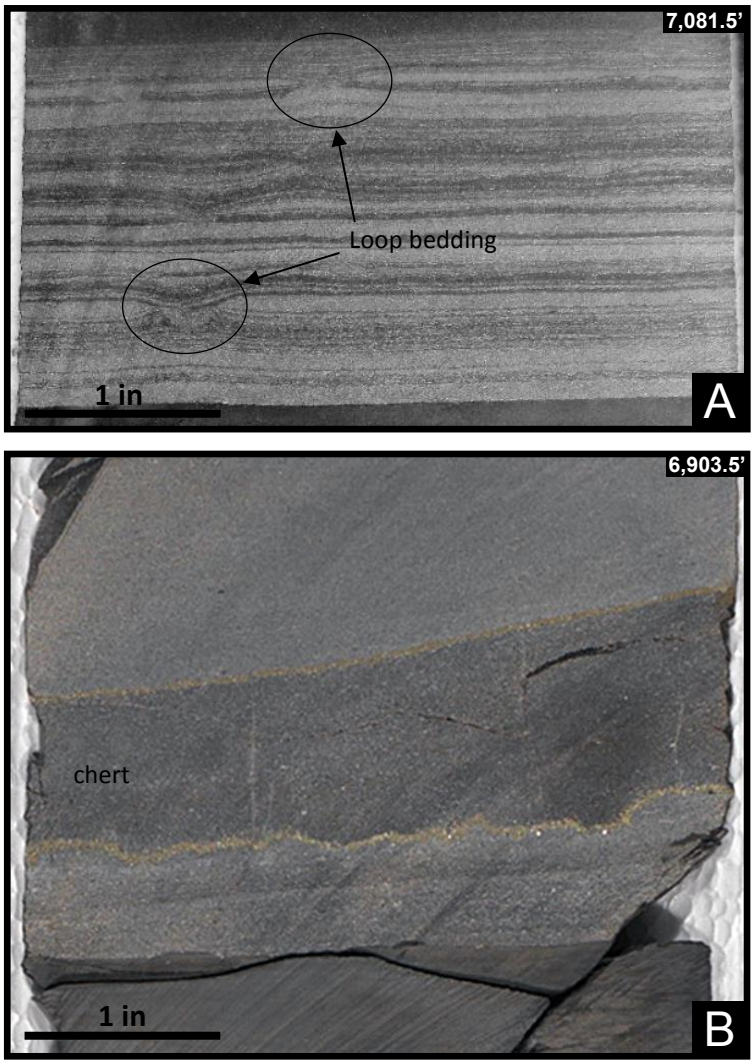

Figure 11. Core photographs of wackestone-packstone. A) Planar laminated wackestone-packstone showing loop bedding. B) Normally graded wackestone-packstone showing chert zone rimmed by pyrite.

DEPOSITIONAL PROCESSES

Wackestone-packstone deposits are interpreted as turbidity current deposits (turbidites) on the basis of the following criteria: sharp basal contacts, normal grading, lamination, and unidirectional current indicators (e.g., low-angle cross-lamination and vergent flame structures) (Bouma, 1962; Walker, 1965; Pickering and Hiscott, 1985; Pickering and Hiscott, 2016). Brachiopods and fusulinids indicate a shallow-water origin.

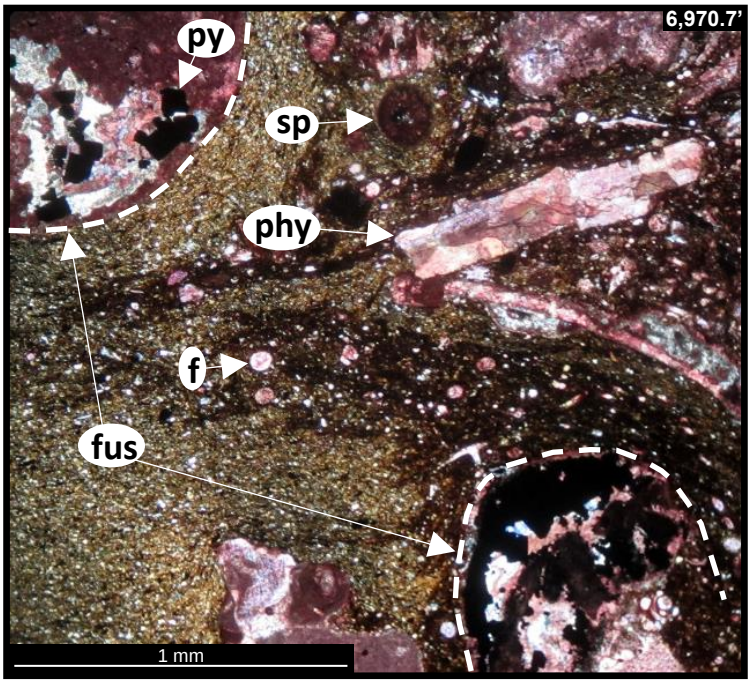

Figure 12. Thin section photomicrograph of wackestone-packstone in cross-polarized light. Alizarin red stain reveals calcareous microfossils scattered in a clay and organic-rich matrix. Pyrite (py) occurs as disseminated grains and as replacement in fusulinids (fus). Other foraminifera (f), phylloid algae (phy), and sponge spicules (sp) are also identified.

Soft sediment deformation (convolute bedding, loop bedding, flame structures) may have resulted from differential compaction or rapid loading by successive gravity flow deposits on unconsolidated sediment.

Many turbidite beds display grading and internal structures consistent with Bouma divisions Ta through Te (Bouma, 1962) (Figure 10); however, complete sequences are uncommon. Thick-bedded wackestone-packstone turbidites (>6 in.) typically have coarse-grained and massive, packstone-dominated lower sections (Ta) indicating rapid fallout from flows with high energy and high sediment concentration. Massive packstone beds are most commonly capped by planar laminated traction deposits composed of finer-grained packstone to wackestone (Tb) and/or mudstone (Te) deposited during flow deceleration. Many thin-bedded turbidites (<6 in.) display planar

and low-angle cross-lamination (Tb and Tc) overlain by thin mudstone layers (Td and/or Te) indicating flows with relatively lower energy and lower sediment concentration. Wackestone without current related structures are interpreted as mixtures of hemipelagic sediment and sediment from waning or dilute turbidity currents.

LITHOFACIES 4. SILTY SANDSTONE

CHARACTERISTICS

Silty sandstone is composed of well-sorted, fine to very fine sand and coarse silt. This lithofacies is identified only in the Dean Formation and is typically interbedded with finer-grained, lithofacies of equal or greater thickness (Figure 4, Appendix). Lower bedding contacts feature sole marks, and upper contacts are sharp or gradational. Normal grading is common around the upper contact of most sandstone beds (Figures 13 and 14). Organic and clay content increase upward in some beds, which darkens the rock. Sandstone is light gray to grayish brown in color, and bed thickness ranges from 1 to 36 in.

Silty sandstone compose a spectrum between thick- and thin-bedded end members. Thick-bedded (>6 in.) sandstone units typically feature a massive lower section overlain by planar lamination and/or bioturbated silt- to clay-size sediment (Figure 13). Planar and low-angle cross-laminae are the defining features of thin beds (<6 in.) (Figure 14). Convoluted bedding was also observed. Many thin bedded silty sandstone are capped by a thin layer of mudstone. Bioturbation is mostly absent except in the upper parts of some thin beds. Trace fossils identified include *Chondrites* and *Phycosiphon* (Figure 14). Other sedimentary features include load casts, current ripple cross-laminae, and flame structures (Figure 14).

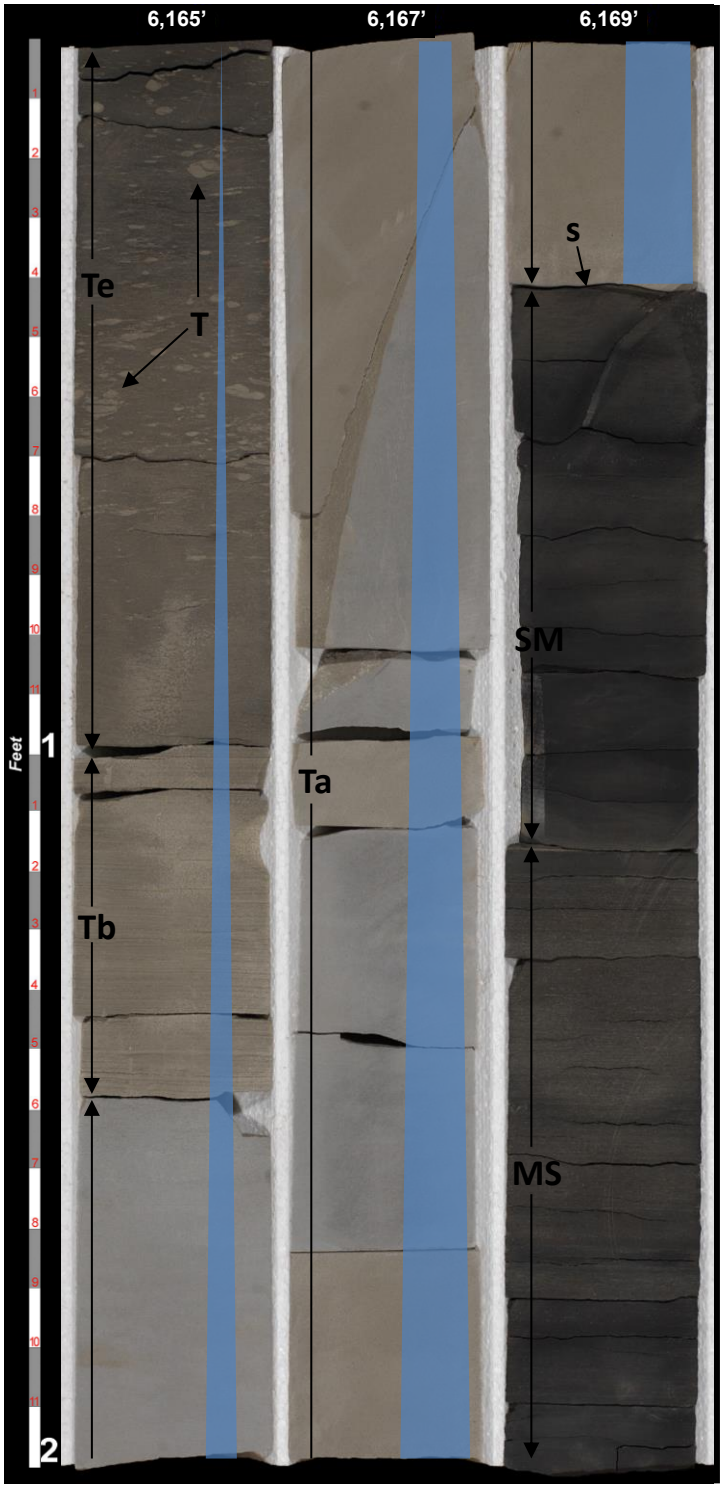

Figure 13. Core Photograph of silty sandstone displaying Bouma divisions Ta, Tb, and Te. Blue triangle represents an overall fining upward sequence. Ta is massive, dolomitic, and fine-grained. Tb is planar-parallel laminated, very fine-grained, and silty. Te is a bioturbated muddy siltstone. The thick, structureless base (Ta) suggests rapid mass deposition due to intergranular friction within a high-density flow. A sole mark (s) is observed at the base of Ta. T = *Teichichnus* burrows; MS = muddy siltstone; SM = siliceous mudstone.

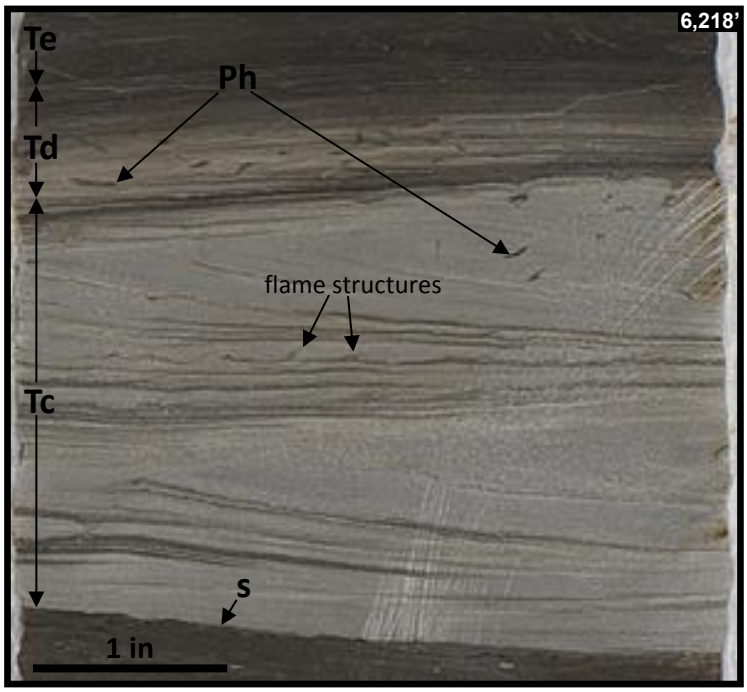

Figure 14. Core photograph of silty sandstone displaying Bouma divisions Tc-e. Tc = very fine-grained, silty sandstone with low-angle cross-lamination. Avalanching and intermittent suspension transport is evident in the alternating coarser and finer grained foresets. Td = silt/mud, planar-parallel lamination. Te = homogenized, silty mudstone cap. Ph = Phycosiphon burrows; s = sole mark..

The grayish brown color of many sandstone beds indicate that dolomite cementation is common (Figure 13). Interparticle dolomite cement observed in thin section supports this observation (Figure 15). Framework grains consist of mostly angular to sub-angular quartz (avg. 59%) and plagioclase (avg. 17%) (Figure 15). Minor amounts of clay and organic matter are present in the sandstone. Pyrite occurs as disseminated, spheroidal framboids.

DEPOSITIONAL PROCESSES

Similar to wackestone-packstone, the silty sandstone lithofacies are also interpreted as turbidites based on vertical successions of current- and traction-generated structures resembling partial Bouma sequences. Evidence of grain-by-grain deposition from evolved currents include size grading, presence of lamination, and cross-

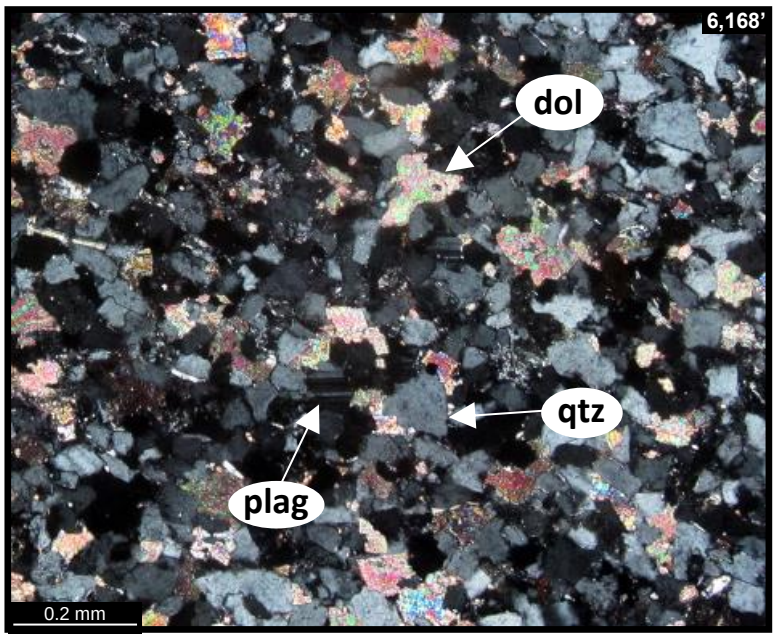

Figure 15. Thin section photomicrograph of silty sandstone sampled from the massive base in Figure 14. Dolomite cement fills the intergranular space between angular to subangular quartz (qtz) and plagioclase (plag).

stratification. Most beds are thin (<6 in.) and typically contain only Bouma's Tc-e divisions suggesting relatively low-energy flows, commonly called distal turbidites. Very thin, planar and lenticular laminations (Td) likely resulted from alternating deposition of sand- to silt-size grains and clay particles by suspension fallout and traction in the bottom boundary layer. The uppermost mud-laden layers (Te) are interpreted to represent the waning stages of turbidity current flow which likely interacted with relatively permanent flows of bottom currents.

LITHOFACIES 5. MUDDY SILTSTONE

CHARACTERISTICS

The muddy siltstone lithofacies most commonly occurs interbedded with mudstone and silty sandstone in the Dean Formation (Figure 4, Appendix). Beds range

from 1 to 48 in. thick and are typically either laminated or intensely and diversely bioturbated (Figures 16 and 17A). Massive bedding occurs locally. Bedding contacts may be sharp or gradational with underlying sandstone and overlying mudstone. Laminated intervals commonly have sharp upper and lower contacts (Figure 16A).

The composition of laminated intervals ranges from light-colored and silt-dominated to dark-colored and clay-rich (Figures 16A and B). Individual laminae also range from silt- to clay-rich (Figure 16A and B). Laminae are typically planar-parallel. Surfaces between laminae appear sharp and continuous or indistinct and discontinuous (Figure 16). Bioturbation (BI = 2-6) is pervasive in this facies, ranging from moderate wherein individual burrows are easily identified, to strong, which is expressed as a mottled texture with few distinct burrows, to beds that are homogenized. Intensely bioturbated beds in places are interbedded with laminated intervals resulting in ill-defined bedding boundaries (Figure 16). Distinct trace fossils identified include *Teichichnus*, *Zoophycos*, *Planolites*, *Chondrites*, and *Phycosiphon* (Figures 16B and 17).

Muddy siltstone consists predominantly of quartz (avg. 47%) and clay (avg. 27%). Silt size ranges from 30-60 µm. Agglutinated foraminifera comprise a portion of the quartz fraction (Figure 18). Clay is predominantly illite-mica and illite-smectite with minor amounts of chlorite. Finely crystalline pyrite (avg. 3.7%) is scattered throughout the matrix and sometimes occurs as a replacement mineral in agglutinated foraminifera (Figure 18). Phosphatic nodules (Figure 17B) are observed in some clay-rich intervals. Average TOC in this facies is 2.36%. Thin sections show that organic matter commonly occurs as bed-parallel strands (Figure 18).

Figure 16. Core photographs of muddy siltstone. A) Light-colored and silt-dominated planar-parallel laminated muddy siltstone underlain by siliceous mudstone (SM). Disrupted laminae in the upper middle portion of the image are the result of bioturbation. B) Dark-colored and clay-rich muddy siltstone overlain by sandstone (Ss). Mottled texture (bottom) and diffuse laminae (top) reflect variation in bioturbation intensity. T = *Teichichnus* (T) burrow.

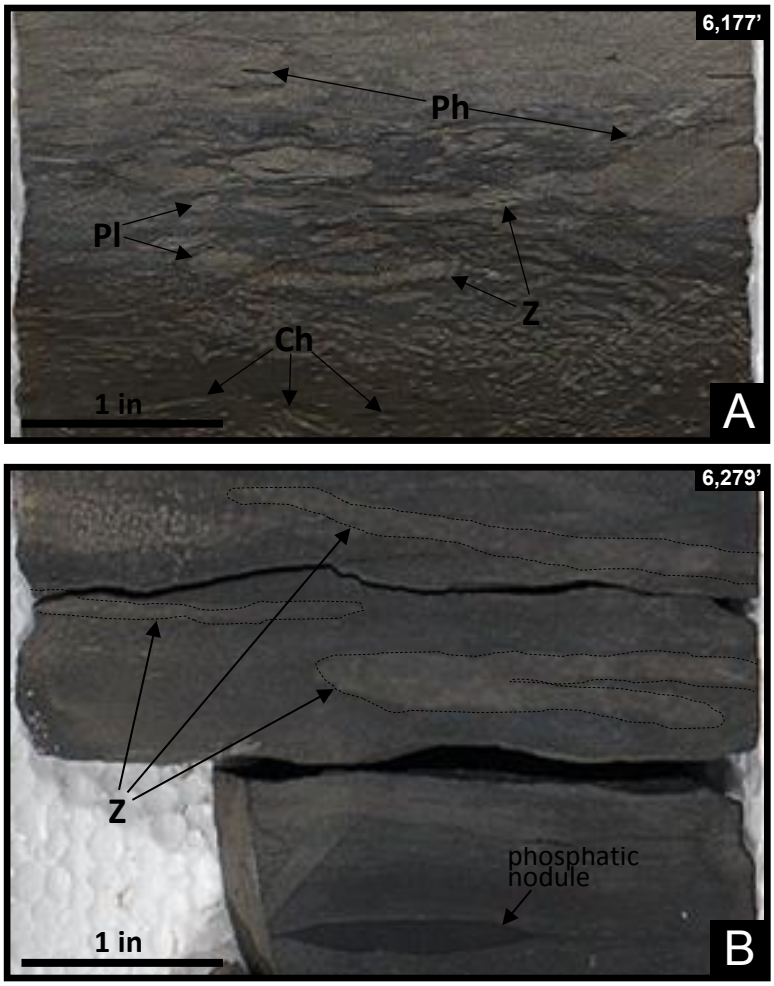

Figure 17. Core photographs of muddy siltstone. A) Intensely bioturbated muddy siltstone. Distinct trace fossils include Phycosiphon (Ph), Planolites (Pl), Zoophycos (Z), and Chondrites (Ch). B) Muddy siltstone showing distinct Zoophycos (Z) burrows and a phosphatic (ph) nodule. In both photos, trace fossils are filled with primarily silt-size sediment.

DEPOSITIONAL PROCESSES

Muddy siltstone are interpreted as predominantly hemipelagic sediments. Hemipelagic deposits (hemipelagites) are formed by settling from dilute suspensions with a low degree of lateral transport in quiescent deep-water environments (Pickering and Hiscott, 2016). Diagnostic features of the muddy siltstone lithofacies include thick sections of structureless muds; alternating very fine silt and clay,

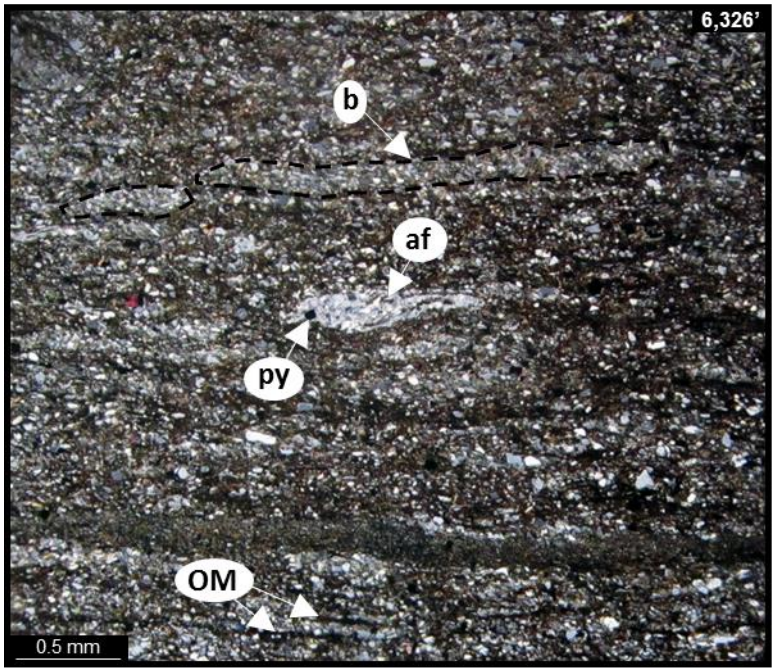

Figure 18. Thin section photomicrograph of muddy siltstone. This bioturbated, muddy siltstone sample consists of quartz (51%), clay (23%), plagioclase (13%), pyrite (py) (4%), and organic matter (OM) (4%). Other distinct features include a clay-rich lamina (bottom), silt-filled burrows (b), and agglutinated foraminifera (af).

parallel laminae; sharp, non-erosive bases; and deep-marine trace fossils, all of which are common features of hemipelagites (Stow and Tabrez, 1998; Shanmugam, 2006).

All trace fossils identified in muddy siltstone are known to be common in deep-water settings (Pickering and Hiscott, 2016). In submarine fan complexes, beds with higher ichnodiversity and bioturbation intensity usually indicate relatively long-term stable conditions between sediment gravity flows and/or in off-axis environments such as channel margins, overbank-levees, and abandoned lobes (Pickering and Hiscott, 2016). Alternating silt- and clay-rich laminae and intervals may indicate alternating energy regimes. Indistinct and discontinuous lamination suggests that some muddy siltstone were deposited or reworked by bottom currents or waning turbidity flows.

LITHOFACIES 6. SILICEOUS TO CALCAREOUS MUDSTONE

CHARACTERISTICS

Siliceous to calcareous mudstone is the dominant lithofacies in the upper Wolfcamp and lower Leonard intervals and occurs interbedded with all other rock types. Siliceous mudstone is dark gray to very dark gray and common throughout the section, whereas calcareous mudstone is relatively lighter gray and more abundant in the lower Leonard (Figure 4, Appendix). These deposits are commonly silty and exhibit massive to weakly laminated or bedded structures reflecting textural and compositional variations. In many places, siliceous and calcareous mudstone occur together in thinly interbedded successions (Figures 19 and 20). Bed thickness ranges from less than 1 in. up to 9 ft. Upper and lower contacts may be sharp or gradational with other facies. Calcareous mudstone commonly have gradational contacts with underlying wackestone-packstone and overlying siliceous mudstone (Figure 20).

Laminae and thin beds are distinguished by slight variations in color and may be lighter or darker than the surrounding mudstone (Figures 19, 20, and 21). Light layers typically comprise higher amounts of silt-size quartz and/or bioclasts. Distinct, light gray carbonate-mud layers are present locally (Figures 19 and 21B). Dark layers are dominated by clay minerals, clay-size quartz, organic matter, and pyrite. Laminae are typically planar-parallel. Wavy and convoluted laminae are visible locally. Laminae bounding surfaces may be sharp, gradational, or diffuse. Discontinuous silt laminae are present locally (Figure 19).

Nodular to elongated, sometimes pyritic, phosphatic nodules are common in siliceous mudstone (Figure 19), and abundant at the base of the lower Leonard. Phosphate is also present in fine-grained laminae (Figure 19). Although less common,

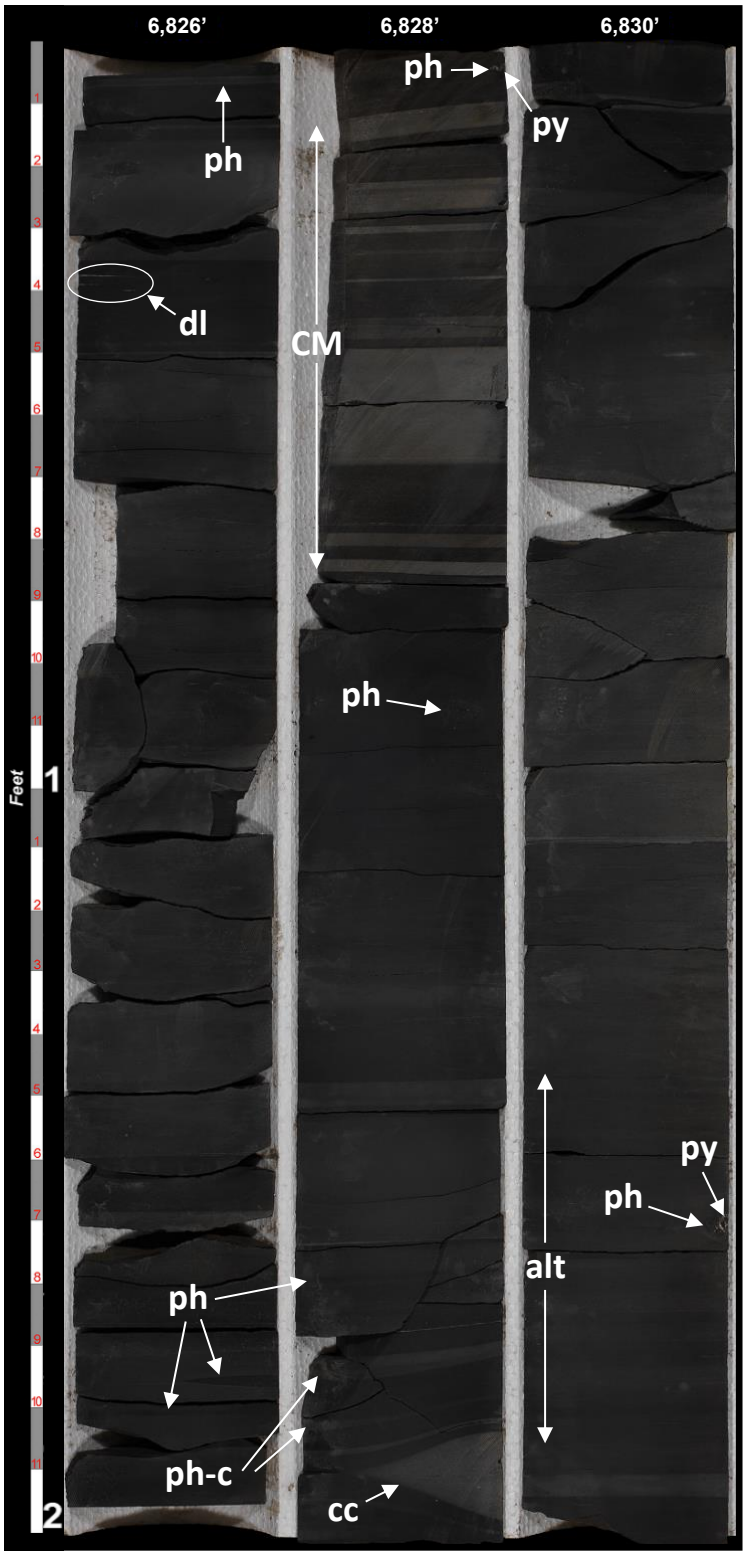

Figure 19. Core photograph showing structureless to weakly bedded siliceous mudstone with distinct interbeds of light gray carbonate mud (CM). Subtle alternation of light and dark layers (alt) reflects variable silt/mud ratios. Phosphate (ph) is present as nodular to elongate nodules and in fine-grained laminae. Other features include discontinuous silt laminae (dl), a carbonate concretion (cc), and pyrite (py) within phosphatic nodules.

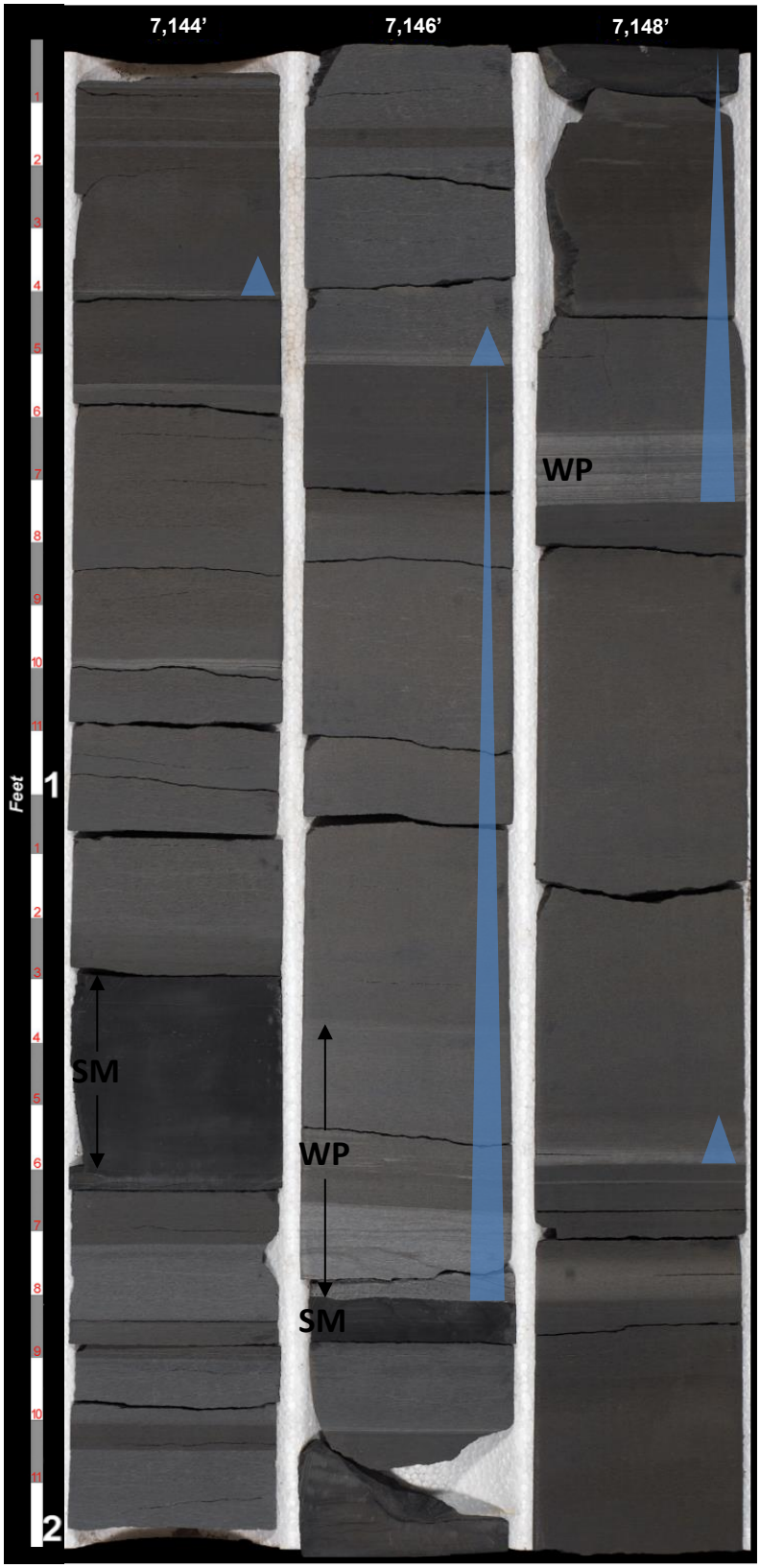

Figure 20. Core photograph showing massive to laminated calcareous mudstone with interbedded wackestone-packstone (WP) and siliceous mudstone (SM). Blue triangles represent fining upward sequences of wackestone packstone to calcareous mudstone.

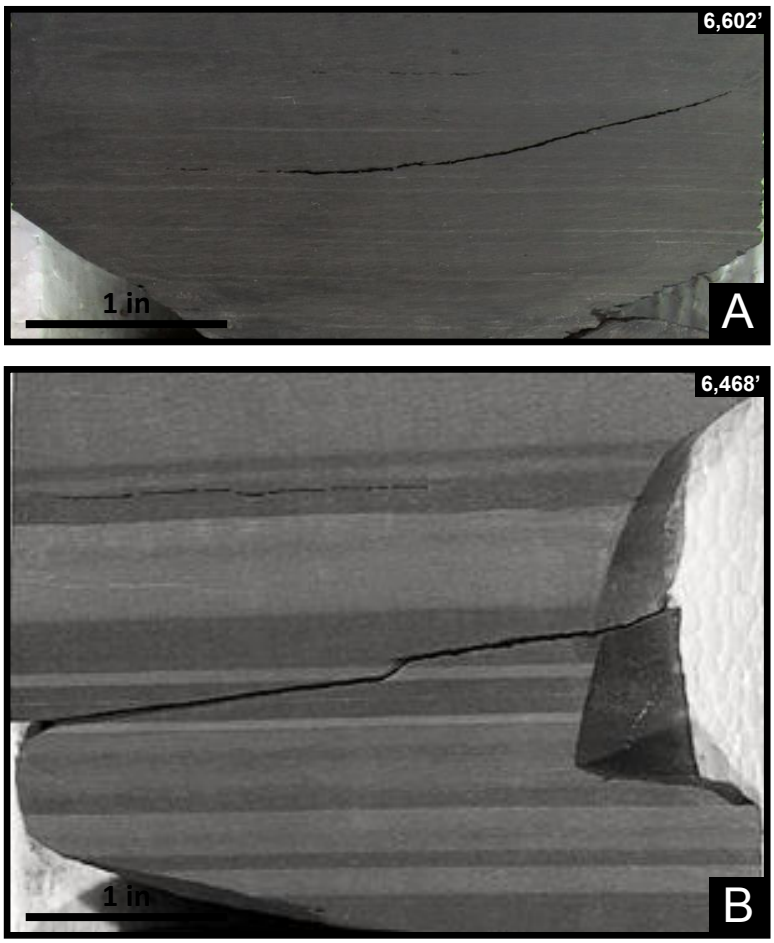

Figure 21. Core photographs of siliceous to calcareous mudstone. A) Faint planar-parallel laminae in siliceous mudstone. Lighter color reflects higher amounts of silt-size quartz grains. B) Thin-bedded calcareous mudstone. Alternating light and dark layers reflect variable carbonate content.

phosphatic nodules are also observed in calcareous mudstone. Pyritic concretions and laminae occur locally in both siliceous and calcareous mudstone. Carbonate concretions up to 3 in. in diameter are identified in some beds (Figure 19). In general, bioturbation is rare. However, large individual burrows recognizable by lighter-colored, more coarse-grained patches are observed in some beds. Distinct trace fossils identified include *Thalassinoides* and *Teichichnus* (Figure 22).

Analyses of thin sections and XRD data show siliceous mudstone contain more quartz (avg. 40%) and clay (avg. 33%) and have higher TOC content (avg. 3.93%) than

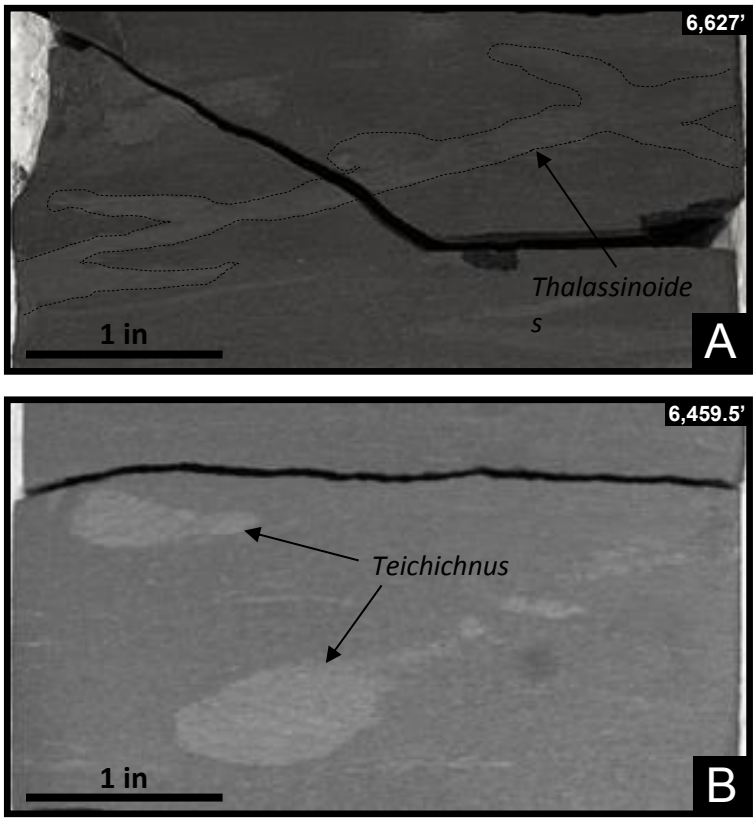

Figure 22. Core photographs of siliceous to calcareous mudstone. A) Thalassinoides burrows in siliceous mudstone. B) Teichichnus burrows in calcareous mudstone.

do calcareous mudstone. Angular to sub-angular, moderately-sorted, clay- to silt-size detrital grains are the most common form of quartz. Diagenetic quartz overgrowths, ellipsoidal peloids, and agglutinated benthic foraminifera (Figure 23A) constitute the remainder of the quartz fraction. Clay aggregates or clusters represent a significant portion of the clay fraction (Figure 23A). Predominant clay phases are illite/mica and illite/smectite. In thin section, pyrite (avg. 4.3%) is present as disseminated, finely crystalline grains and clusters of grains or framboids (Figure 23A). Sparse skeletal fragments were also identified is siliceous mudstone.

Calcareous mudstone contain more carbonate (avg. 49%) than do siliceous mudstone. Calcite is present in the forms of interparticle cement, thin micritic laminae,

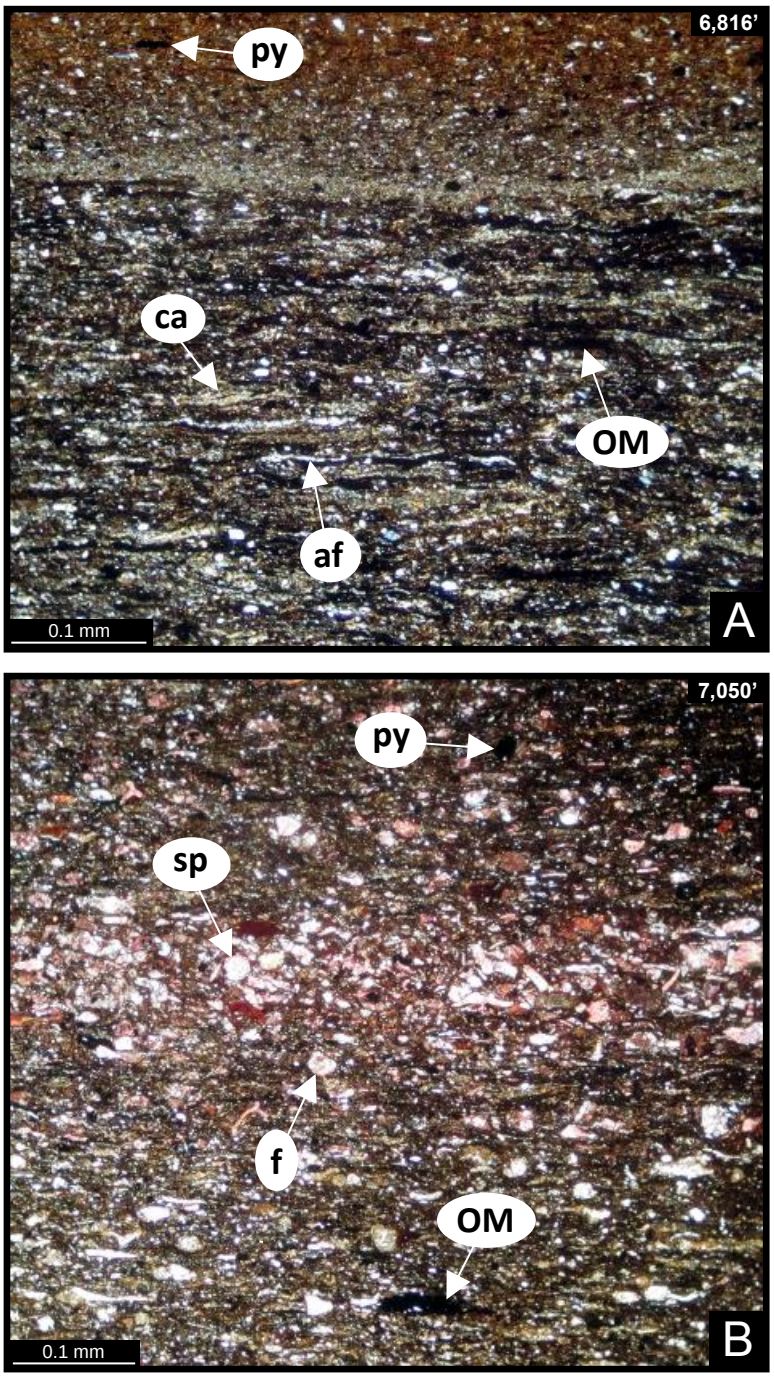

Figure 23. Thin section photomicrographs of siliceous to calcareous mudstone. A) Siliceous mudstone: a thin, clay-rich interval separates a phosphatic layer (top) from an organic-rich layer (bottom). Composition is dominated by clay aggregates (ca), agglutinated foraminifera (af), strands of organic matter (OM), pyrite (py), and silt-sized quartz grains. B) Calcareous mudstone: alizarin red stain reveals that calcite is present as calcite-replaced foraminifera (f), sponge spicules (sp), and other skeletal grains. Clusters of pyrite (py) and relatively large strands of organic matter (OM) are scattered throughout this sample.

and scattered microfossils. Fossils include benthic foraminifera tests, sponge spicules, and skeletal debris (Figure 23B). Tabular skeletal fragments sometimes highlight the laminated fabric. Dolomitization of microfossils and interparticle dolomite cement was observed in some samples. Pyrite (avg. 3.7%) appears as clusters of grains and occasionally as a replacement mineral in microfossils (Figure 23B). Average TOC content in calcareous mudstone is 2.81%. Organic matter occurs as disseminated matrix material and scattered bed-parallel strands (Figure 23B).

DEPOSITIONAL PROCESSES

Based on the predominance of clay-size particles and massive to weakly laminated or thin-bedded structures, siliceous to calcareous mudstone are interpreted as predominantly hemipelagic sediments. Subtle textural and compositional variations are considered to be the result of fluctuations in terrigenous and biogenic input. As with muddy siltstone, local wavy to discontinuous laminae indicate that mudstone were sometimes deposited or reworked by bottom current processes. Furthermore, in calcareous mudstone, gradational lower contacts with coarser grained lithologies are common and interpreted as deposition during the waning stages of sediment gravity flows. Locally visible soft sediment deformation (convolute laminae) appear to be post-depositional and likely resulted from rapid loading by gravity flow deposits.

Current-generated sedimentary structures are rare suggesting that these sediments settled out of suspension mostly in low-energy settings. *Thalassinoides* and *Teichichnus* are common deep-water, ichnofabric-forming trace fossils which imply quiet water conditions (Pickering and Hiscott, 2016). The abundance of phosphatic nodules in siliceous mudstone indicates low rates of deposition and reduced clastic and carbonate supply (Jarvis et al., 1994).

CHAPTER V

DISCUSSION

DEPOSITIONAL SYNTHESIS

Using lithofacies observations, relationships, and inferred depositional processes, this section provides an interpretation of the depositional conditions that existed during formation of the upper Wolfcamp-Dean interval. Siliceous to calcareous mudstone and muddy siltstone represent predominantly hemipelagic sediment deposited in low-energy settings. Hemipelagic sedimentation was interrupted episodically by rapid deposition of relatively coarse-grained, carbonate-rich grain, debris, and turbidity flows. Skeletal-dominated packstone-grainstone (grain flows), muddy bioclastic-lithoclastic floatstone-rudstone (debrites), and skeletal-argillaceous wackestone-packstone (turbidites) consisting of shallow-water and reef-forming biota were transported from adjacent shelf areas. Soft sediment deformation (flame structures, convolute laminae, loop bedding, microfaults) occurred locally and are interpreted as a result of differential compaction, dewatering, and rapid loading by gravity flow deposits on underlying unconsolidated sediment. Following gravity flows, finely disintegrated carbonate material was carried into the basin and settled out of suspension, mixing with background hemipelagic sediment and producing calcareous wackestone to mudstone that grade upward into siliceous mudstone. Slowly accumulating hemipelagic sediment, primarily siliceous mudstone, defined the system until the next gravity flow.

A similar depositional pattern occurs in the Dean Formation; however, gravity flow deposits are dominated by siliciclastic strata. Silty sandstone was transported to the basin by turbidity currents that grade upward into laminated and/or bioturbated muddy siltstone and siliceous mudstone, which constitute the hemipelagic component of the system.

Estimates of maximum water depth in the Midland Basin during Wolfcampian-Leonardian time range from 1,000 ft. in the early Wolfcampian (Hobson et al., 1985) to 2,000 ft. in the early Leonardian (Montgomery, 1996). Several lines of evidence indicate that these facies accumulated under dominantly deep water reducing conditions including high organic content (up to 8% locally) (Sageman et al., 2003), widespread abundance of pyrite (Wignall et al., 2010), and prevalence of phosphatic nodules (Jarvis et al., 1994) in many clay-rich intervals. Agglutinated foraminifera were commonly observed in siliceous mudstone and muddy siltstone and are known to survive under dysoxic to anoxic conditions (Sen Gupta and Machain-Castillo, 1993). Furthermore, all trace fossils identified in the study core are apparently common in deep water settings deficient in oxygen (Pickering and Hiscott, 2016).

A depositional model for the Midland Basin during Wolfcampian-Leonardian time is shown in Figure 24. Based on the mixture of mud-dominated and grain-dominated fabrics, high organic content and laminated character of mud-rich facies, abundance of pyrite and phosphatic nodules, deep-water trace fossil assemblages, and frequency of gravity-driven sedimentary structures in coarse-grained sediments, it is interpreted that deposition occurred in a deep water dysoxic to anoxic, distal toe-of-slope to basin plain setting where hemipelagic sedimentation was interrupted by periodic gravity flow deposition.

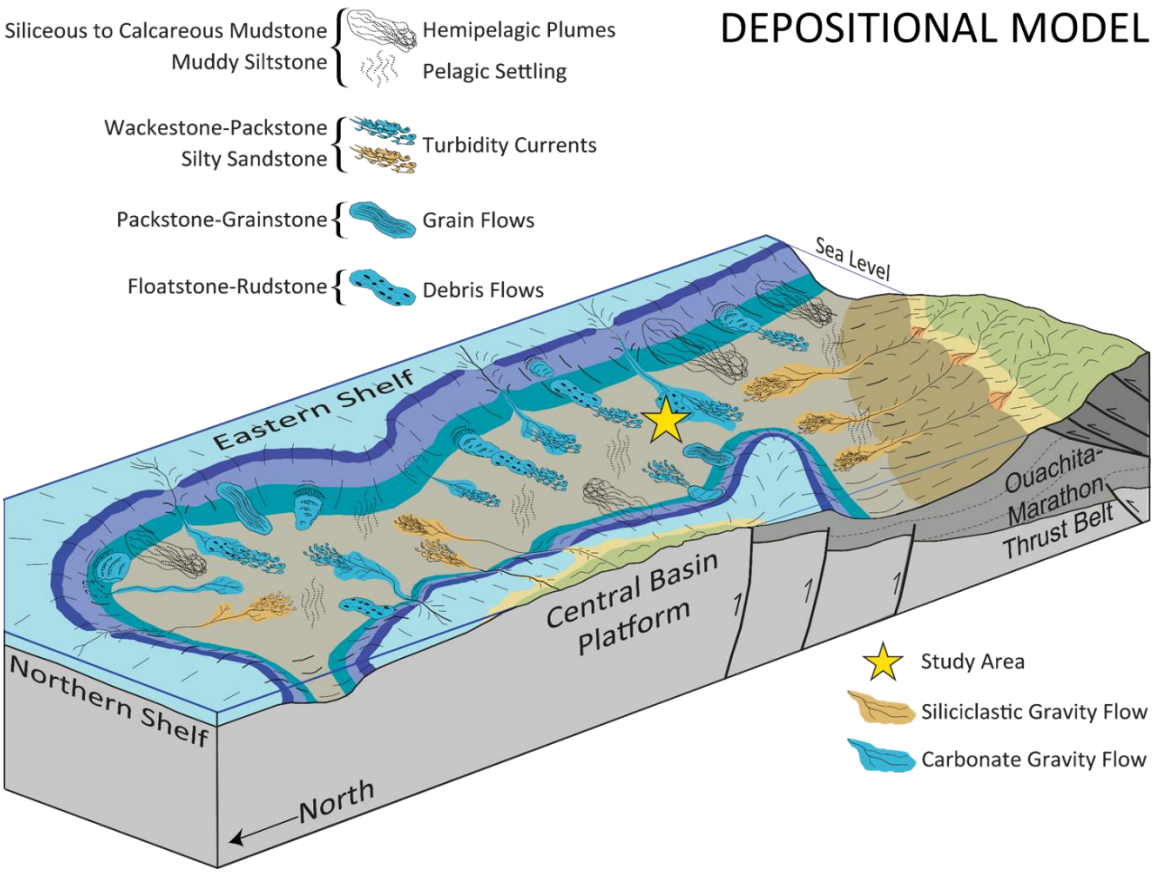

Figure 24. Envisioned depositional model for the Midland Basin during Wolfcampian-Leonardian time. Modified from Hanford, 1981; Pioneer Natural Resources, 2013.

SEQUENCE STRATIGRAPHIC INTERPRETATION

A lack of physical connection or continuous data connection between shallow and deep-water systems can make deep-water deposits difficult to interpret in sequence stratigraphic terms; however, expected changes in the frequency and type of gravity flows that operate during consecutive stages of a base-level cycle allow these sediments to be studied, at least to some extent, within the predictive framework of sequence stratigraphy (Catuneanu, 2006). Historically, the Northern Platform of the Midland Basin has been given much attention with regard to correlating cyclic shelf carbonates to mixed siliciclastics and detrital carbonates deposited in the basin; and the depositional

framework of the Northern Platform is grossly similar to that of the Eastern Shelf of the southern Midland Basin (Mazzullo and Reid, 1989). To test for conformance with previous interpretation, the relative sea level curve proposed by Mazzullo and Reid (1989) is superimposed, and age-calibrated (stretched), on the succession of facies and flow processes interpreted in this study (Figure 25).

Individual, upward-fining cycles of gravity flow deposits overlain by hemipelagic sediments are the fundamental units of deposition in basinal upper Wolfcamp and lower Leonard strata. Gravity flow deposits represent three primary modes of deposition: grain flows, debris flows, and turbidity currents (Figure 25). High- to low-density turbidites are common throughout most of the upper Wolfcamp-lower Leonard interval, most notably in the lower Leonard. Grain flow and debris flow deposits are much less common and occur in the upper Wolfcamp only. The presence of shelf-derived bioclasts in these allochthonous sediments suggests that carbonate shelf margins were eroded periodically. High-frequency glacial eustatic sea level fluctuations were probably responsible for erosion on the margin, and thus for the cycles observed in this study.

Late Wolfcampian-early Leonardian sedimentation occurred during a period of waning icehouse conditions resulting in long-term sea level rise punctuated by high-amplitude and high-frequency eustatic fluctuations (Rygel et al., 2008; Holterhoff, 2010; Wahlman and Tasker, 2013). In late Wolfcampian time, highstands were followed by progressively higher highstands interrupted by relatively minor lowstands (Mazzullo and Reid, 1989, Wahlman and Tasker, 2013). Development of shelves around the Midland Basin corresponded to these sea level changes by aggrading and backstepping. This can be seen on the Central Basin Platform, where upper Wolfcamp platform carbonates are overlain by lower Leonard basinal shales (Wahlman and Tasker, 2013). Cycles of sea level rise and fall are preserved on the Eastern Shelf in packages of marine

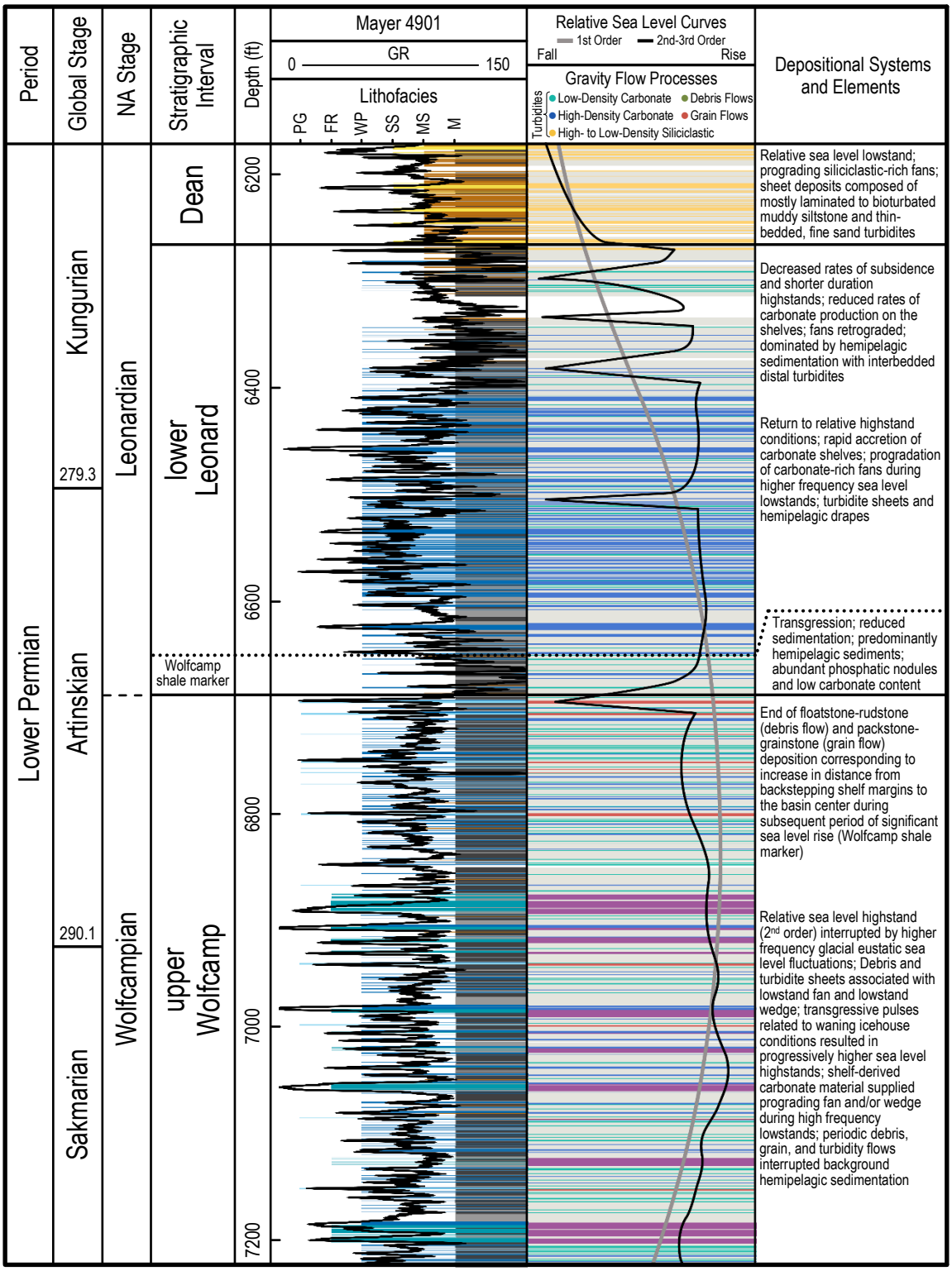

Figure 25. Summary of inferred depositional systems within the upper Wolfcamp, lower Leonard, and Dean stratigraphic intervals. Calibrated gamma ray signature is plotted on top of lithofacies column. Relative eustatic sea level change curves for the Midland Basin proposed by Mazzullo and Reid (1989) are plotted on top of interpreted gravity flow processes for visual comparison.

carbonates overlying coastal-plain sediments (Holterhoff, 2010). In basinal settings, sea level fall has been attributed to allochthonous carbonates produced by erosional backstepping shelves (Mazzullo, 1995) and incising valleys (Morgan et al., 1996). Thick debris flow deposits are likely a result of major, episodic events in which large sections of adjacent shelves collapsed in response to periods of relative sea level lowstand (Mazzullo and Reid, 1989; Hamlin and Baumgardner, 2012). Hobson et al (1985) interpreted basin-floor floatstone-rudstone (conglomerates and breccias) as episodic debris flow sheet complexes and were able to correlate them tens of miles across the southern Midland Basin. In a more distal location, debris flow deposits (floatstone-rudstone) in this study likely represent the muddier, finer-grained, distal equivalents of those in their study.

Following a relatively minor unconformity that marks the end of Wolfcampian time (Wahlman and Tasker, 2013), sea level rise continued. A period of rapid sea-level rise immediately following the latest Wolfcampian unconformity (Mazzullo et al., 1987) is marked by a high gamma ray spike (Wolfcamp shale marker) (Figure 25) and characterized in core by abundant phosphatic nodules and low carbonate content. Carbonate gravity flow deposition in the basin center all but ceased during this period.

In the lower Leonardian section, the absence of grain flow and debris flow deposits and an increase in abundance of high- and low-density carbonate turbidites (Figure 25) suggests that carbonate shelf margins had backstepped a considerable distance from the study area. Relatively low-density, fine-grained turbidites represent deposition of sediments at the greatest distance from the shelf margin. Continued transgression in the early Leonardian resulted in aggradation and backstepping of carbonate shelf margins (Wahlman and Tasker, 2013), as evidenced on the eastern margin of the Central Basin Platform where upper Wolfcamp platform carbonates are

seen overlain by lower Leonard basinal shales (Wahlman and Tasker, 2013). Mazzullo and Reid (1989) attribute the abundance of carbonates in the lower Leonard to 1) great thickness of shelf margin reefs, 2) considerable shelf to basin relief, 3) steep fore-reef slopes that provided a constant supply of carbonate debris to the basin, and 4) increased accommodation due to rapid basin subsidence.

The Tubb Formation is the shelfal equivalent of the Dean Formation. The Tubb Formation consists of sandstones, anhydritic shale, evaporites, and shallow marine dolomites (Hobson et al., 1985; Mazzullo and Reid, 1989) deposited during a time of gradual sea level fall, which ultimately resulted in complete shelf emergence (Silver and Todd, 1969). Multiple small-scale cycles of sea level change are recorded in these in shelf deposits (Mazzullo and Reid, 1989).

In this study, the Dean interval is characterized by silty sandstone turbidites interspersed throughout a hemipelagic, muddy siltstone-dominated succession (Figure 25). According to Tyler et al. (1997), Dean Formation depositional systems are composed of turbidite-channel and –lobe depositional elements enclosed in laterally extensive turbidite sheets and hemipelagic drapes. Thick-bedded turbidites form mainly in channels and lobes, whereas thin-bedded turbidites are typically deposited in more distal sheet complexes. The dominantly thin-bedded nature of siliciclastic turbidites observed in in this study indicate a distal lobe fringe setting.

Gravity flows in deep-water settings may occur throughout the full cycle of base level changes (Catuneanu, 2006); however, the vast majority of these flows are deposited as part of a lowstand fan and/or lowstand wedge (Posamentier and Vail, 1988). The presence of cycles both in the basin and on carbonate shelves suggests that basinal sediment may have been deposited as a result of the same high-frequency sea

level changes interpreted in shallow-water settings; however, gravity flow deposits that define the base of these cycles apparently constitute solitary events.

CHAPTER VI

CONCLUSIONS

Basinal strata of the late Wolfcampian to early Leonardian succession in the southern Midland Basin are composed of resedimented siliciclastic- and carbonate-rich lithofacies. The upper Wolfcamp is dominated by siliceous mudstone delivered to the basin floor by hemipelagic settling. Siliceous mudstone are interbedded with various types of carbonate gravity flow deposits that originated along the basin margins, including packstone-grainstone (grain flows), floatstone-rudstone (debris flows), and wackestone-packstone (turbidity currents). In the lower Leonard, calcareous mudstone is more common and interbedded with abundant wackestone-packstone turbidites. The Dean Formation is dominated by hemipelagic muddy siltstone with interbedded silty sandstone deposited by turbidity currents.

Gravity flow deposits were transported to the basin primarily during relative sea level lowstands as sheet deposits. Cyclicity is evident in individual upward-fining trends of floatstone-rudstone or wackestone-packstone overlain by calcareous and siliceous mudstone. Cycles reflect high-frequency, sea level-driven cyclicity on surrounding shallow-water shelves. Cessation of mass-transport deposits (grain flows and debris flows) in latest Wolfcampian time coincides with significant relative sea level rise and increased distance from backstepping margins to the basin center.

These strata were deposited in deep water dysoxic to anoxic conditions most of the time, inhibiting bottom-dwelling infauna and preserving organic matter. TOC is facies-dependent and vertically discontinuous. Periodic downslope transport of organic matter-poor carbonate debris interrupted background hemipelagic sedimentation and accumulation of organic matter. Siliceous mudstone have the highest average TOC (3.93%), followed by calcareous mudstone (2.81%) and muddy siltstone (2.36%).

.

REFERENCES

Adams, J.E., Cheney, M.G., DeFord, R.K., Dickey, R.I., Dunbar, C.O., Hills, J.M., King, R.E., Lloyd, E.R., Miller, A.K. & Needham, C.E., 1939, Standard Permian section of North America: AAPG Bulletin, v. 23, p. 1673-1681.

Adams, J.E., 1965, Stratigraphic-tectonic development of Delaware Basin: AAPG Bulletin, v. 49, p. 2140-2148.

Asmus J.J. & Grammer G.M., 2013, Characterization of deep-water carbonate turbidites and mass-transport deposits utilizing high-resolution electrical borehole image logs: Upper Leonardian (Lower Permian) Upper Bone Spring Limestone, Delaware Basin, Southeast New Mexico and West Texas: Gulf Coast Association of Geological Societies, Transactions, v. 63, p. 27-65.

Bann, K.L., Tye, S.C., MacEachern, J.A., Fielding, C.R. & Jones, B.G., 2008, Ichnological signatures and sedimentology of mixed wave- and storm-dominated deltaic deposits: Examples from the Early Permian, southern Sydney Basin of southeastern Australia, in Hampson, G., Steel, R., Burgess, P. & Dalrymple, R., eds., Recent advances in models of siliciclastic shallow-marine stratigraphy: SEPM Special Publication 90, p. 293-332.

Baumgardner, R.W., Jr., Hamlin, H.S. & Rowe, H.D., 2014, High-resolution core studies of Wolfcamp/Leonard basinal facies, southern Midland Basin, Texas: Southwest Section AAPG, 2014 Annual Convention: West Texas Geological Society Publication no. 14-127, v. 1, p. 38-39.

Beckwith, R., 2013, Tight resources, promising economics: The Permian Basin continues yielding liquid riches: Journal of Petroleum Technology, February 2013, p. 54-58.

Bouma, Arnold H., 1962, Sedimentology of some flysch deposits: A graphic approach to facies interpretation: Amsterdam, Elsevier, 168 p.

Candelaria, M.P., Sarg, J.F., & Wilde, G.L., 1992, Wolfcamp sequence stratigraphy of the eastern Central Basin Platform, in Mruk, D.H. & Curran, C., eds., Permian Basin exploration and production strategies: Application of sequence stratigraphic and reservoir characterization concepts: West Texas Geological Society Publication, v. 92-91, p. 27-44.

Catuneanu, O., 2006, Principles of sequence stratigraphy: Amsterdam, Elsevier, 375 p.

Cys, J.M. & Gibson, W.R., 1988, Pennsylvanian and Permian geology of the Permian Basin region, in Sloss, L.L., ed., Sedimentary cover— North American craton, U.S.: Boulder, Colorado, Geological Society of America, The Geology of North America, v. D-2, p. 277-289.

Crevello, P.D. & Schlager, W., 1980, Carbonate debris sheets and turbidites, Exuma Sound, Bahamas: Journal of Sedimentary Petrology, v. 50, p. 1121-1148. Cook, H.E., 1983, Sedimentology of some allochthonous deepwater carbonate reservoirs, Lower Permian, west Texas: Carbonate debris sheets, aprons, or submarine fans?: AAPG Bulletin, v. 63, p. 442.

Dunham, R.J., 1962, Classification of carbonate rocks according to depositional texture, in Ham, W.E., ed., Classification of carbonate rocks: AAPG Memoir 1, p. 108-121.

Fielding, C.R., Frank, T.D. & Isbell, J.L., 2008, The late Paleozoic ice age—A review of current understanding and synthesis of global climate patterns, in Fielding, C.R., Frank, T.D. & Isbell, J.L., eds., Resolving the Late Paleozoic Ice Age in time and space: Geological Society of America Special Paper no. 441, p. 343-354.

Fitchen, W., 1997, Lower Permian sequence stratigraphy of the western Delaware Basin margin, Sierra Diablo, west Texas: Ph.D. dissertation, The University of Texas at Austin, 264 p.

Fitchen, W., Starcher, M.A., Buffler, R.T., & Wilde, G.L., 1995, Sequence stratigraphic framework of the Lower Permian carbonate platform margins, Sierra Diablo, west Texas, in Garber, R.A. & Lindsay, R.F., eds., Wolfcampian–Leonardian shelf margin facies of the Sierra Diablo— Seismic scale and models for subsurface exploration: West Texas Geological Society Publication no. 95-97, p. 23-66.

Flamm, D.S., 2008, Wolfcampian development of the nose of the Eastern Shelf of the Midland Basin, Glasscock, Sterling, and Reagan Counties, Texas: Master's thesis, Brigham Young University, 54 p.

Hamlin, H.S. & Baumgardner, R.W., 2012, Wolfberry (Wolfcampian-Leonardian) deep-water depositional systems in the Midland Basin: Stratigraphy, lithofacies, reservoirs, and source rocks: Report of Investigations 277, Bureau of Economic Geology, The University of Texas at Austin, 61 p.

Hanford, C.R., 1981b, Coastal sabkha and salt pan deposition of the lower Clear Fork Formation (Permian), Texas: Journal of Sedimentary Petrology, v. 51, p. 761-778.

Harris, D.G. & Sarg, J.F., 1989, Seismic modeling of a mixed carbonate-siliciclastic prograded system, Middle Permian, Permian Basin, in Flis, J.E., Price, R.C. & Sarg, J.F., eds., Search for the subtle trap - hydrocarbon exploration in mature basins: West Texas Geological Society Publication no. 89-85, p. 119-138.

Heckel, P.H., 1977, Origin of phosphatic black shale facies in Pennsylvanian cyclothems of midcontinent North America: AAPG Bulletin, v. 61, p. 1045-1068.

Heckel, P.H., 1986, Sea-level curve for Pennsylvanian eustatic marine transgressive-regressive depositional cycles along midcontinent outcrop belt, North America: Geology, v. 14, p. 330-334.

Henderson, C.M., Davydov, V.I. & Wardlaw, B.W., 2012, The Permian Period, in Gradstein, F.M., Ogg, J.G., Schmitz, M.D. & Ogg, G.M., eds., The geologic time scale 2012: Oxford, Elsevier, p. 652-679.

Hills, J.M., 1972, Late Paleozoic sedimentation in west Texas Permian Basin: AAPG Bulletin, v. 56, p. 2303-2322.

Hills, J.M., 1984, Sedimentation, tectonism, and hydrocarbon generation in Delaware Basin, west Texas and southeastern New Mexico: AAPG Bulletin, v. 68, p. 250-267.

Hobson, J.P., Jr., Caldwell, C.D. & Toomey, D.E., 1985, Early Permian deep-water allochthonous limestone facies and reservoir, West Texas: AAPG Bulletin, v. 69, p. 93-139.

Holterhoff, P., 2010, Sequence stratigraphy and depositional systems of Eastern Shelf Lower Permian, central Texas: examining the tropical record of late Paleozoic climate change: SEPM field trip guidebook, Permian Basin Section: SEPM Publication No. 10–50, unpaginated.

Horak, R.L., 1985, Tectonic and hydrocarbon maturation history in the Permian Basin: Oil and Gas Journal, v. 83, no. 21, p. 124-129.

Janson, X., Kerans, C., Bellian, J.A. & Fitchen, W., 2007, Three-dimensional geological and synthetic seismic model of Early Permian redeposited basinal carbonate deposits, Victorio Canyon, west Texas: AAPG Bulletin, v. 91, p. 1405-1436.

Jarvis, I., Burnett, W.C., Nathan, Y., Almbaydin, F.S.M., Attia, A.K.M., Castro, L.N., Flicoteaux, R., Hilmy, M.E., Husain, V., Qutawnah, A.A., Serjani, A. & Zanin, Y.N., 1994, Phosphorite geochemistry: state-of-the-art and environmental concerns: Ecologae Geologicae Helvetiae, v. 87, no. 3, p. 643-700.

Lazar, O.M., Bohacs, K.M., Macquaker, J.H.S., Schieber, J. & Demko, T., 2015, Capturing key attributes of fine-grained sedimentary rocks in outcrops, cores, and thin sections: Nomenclature and description guidelines: Journal of Sedimentary Research, v. 85, p. 230-246.

Lowe, D.R., 1976a, Grain flow and grain flow deposits: Journal of Sedimentary Petrology, v. 46, p. 188-199.

Lowe, D.R., 1982, Sediment gravity flows: II. Depositional models with special reference to the deposits of high-density turbidity currents: Journal of Sedimentary Petrology, v. 52, p. 279-297.

Mazzullo, S.J., 1995, Permian stratigraphy and facies, Permian Basin (Texas-New Mexico) and adjoining areas in the Midcontinent United States, in Scholle, P.A., Peryt, T.M. & Ulmer-Scholle, D.S., eds., The Permian of Northern Pangea: New York, Springer-Verlag, v. 2, p. 41–60.

Mazzullo, S.J. & Reid, S.T., 1987, Contrasting evolutionary patterns of Lower Permian shelf and basinal facies, Midland Basin, Texas: AAPG Bulletin, v. 71, p. 590-591.

Mazzullo, S.J. & Reid, A.M., 1988, Stratigraphic architecture of Pennsylvanian and Lower Permian facies, northern Midland Basin, Texas, in Cunningham, B.K., ed., Permian and Pennsylvanian stratigraphy, Midland Basin, west Texas: Studies to aid hydrocarbon exploration: SEPM Publication, Permian Basin Chapter, v. 88-28, p. 1-6.

Mazzullo, S.J. & Reid, A.M., 1989, Lower Permian platform and basin depositional systems, northern Midland basin, Texas, in Crevello, P.D., Wilson, J.L., Sarg, J.F. & Read, J.F., eds., Controls on carbonate platform and basin development: SEPM Special Publication 44, p. 305-320.

Mazzullo, S.J. & Montgomery, S.L., 1997, Permian 'Wolfcamp' limestone reservoirs, Powell Ranch Field, eastern Midland Basin; discussion and reply: AAPG Bulletin, v. 81, no. 10, p. 1750-1755.

Middleton, G.V. & Hampton, M.A., 1976, Sediment gravity flows: Mechanics of flow and deposition, in Middleton, G.V. & Bouma, A.H., eds., Turbidites and deep water sedimentation: SEPM, Pacific Section short course lecture notes, p. 1-38.

Miller, C., Hamilton, D., Sturm, S., Waters, G., Taylor, T., Le Calvez, J. & Singh, M., 2013, Evaluating the impact of mineralogy, natural fractures, and in-situ stresses on hydraulically-induced fracture system geometry in horizontal shale wells: SPE Paper 163878, presented at the SPE Hydraulic Fracturing Technology Conference, The Woodlands, Texas, February 4-6, 2013.

Montgomery, S.L., 1996, Permian 'Wolfcamp' limestone reservoirs; Powell Ranch Field, eastern Midland Basin: AAPG Bulletin, v. 80, p. 1349-1365.

Morgan, W.A., Clopine, W.W., Kokkoros, G.F. & Wiley, B.H., 1996, Sequence stratigraphic framework and exploration potential of lower Permian (Wolfcampian) gravity-flow deposits, eastern Midland Basin, Texas: AAPG-SEPM Annual Meeting, Abstracts, v. 5, p. 101.

Mulder, T. & Alexander, J., 2001, The physical character of subaqueous sedimentary density flows and their deposits: Journal of Sedimentology, v. 48, p. 269-299.

Mullins, H.T. & Cook, H.E., 1986, Carbonate apron models: Alternatives to the submarine fan model for paleoenvironmental analysis and hydrocarbon exploration: Sedimentary Geology, v. 48, no. 1-2, p. 37-79.

Owen, G., Moretti, M. & Alfaro, P., 2011, Recognising triggers for soft-sediment deformation: Current understanding and future directions: Sedimentary Geology, v. 235, no. 3-4, p. 133-140.

Pacht, J.A., Brooks, L. & Messa, F., 1995, Stratigraphic analysis of 3D and 2D seismic data to delineate porous carbonate debris flows in Permian strata along the northwestern and eastern margins of the Midland Basin, in Martin, R.L., ed., In search of new Permian Basin oil and gas fields: Using today's technologies and tomorrow's ideas for exploration, development, and 3D seismic in a mature basin: West Texas Geological Society Publication no. 95-98, p. 83-86.

Pashin, J.C. & Ettensohn, F.R., 1992, Palaeoecology and sedimentology of the dysaerobic Bedford fauna (late Devonian), Ohio and Kentucky (USA): Palaeogeography, Palaeoclimatology, Palaeoecology, v. 91, no. 1-2, p. 21-34.

Pashin, J.C., Kopaska-Merkel, D.C., Arnold, A.C. & McIntyre, M.R, 2011, Geological foundation for production of natural gas from diverse shale formations: Research Partnership to Secure Energy for America (RPSEA) Final Report 0712217.01, 156 p.

Pickering, K.T. & Hiscott, R.N., 1985, Contained (reflected) turbidity currents from the Middle Ordovician Cloridorme Formation, Quebec, Canada: An alternative to the antidune hypothesis: Sedimentology, v. 32, p. 373-394.

Pickering, K.T. & Hiscott, R.N., 2016, Deep marine systems: processes, deposits, environments, tectonics and sedimentation: John Wiley & Sons, Chichester, West Sussex, UK; Hoboken, New Jersey, USA, 657 p.

Playton, T. & Kerans, C., 2002, Slope and toe-of-slope deposits shed from a late Wolfcampian tectonically active carbonate ramp margin: Gulf Coast Association of Geological Societies, Transactions, v. 52, p. 811-820.

Posamentier, H.W. & Martinsen, O.J., 2011, The character and genesis of submarine mass-transport deposits: Insights from outcrop and 3D seismic data, in Shipp, R.C., Weimer, P. & Posamentier, H.W., eds., Mass-transport deposits in deepwater settings: SEPM Special Publication 96, p. 7-38.

Potter, P.E., Maynard, J.B. & Pryor, W.A., 1980, Sedimentology of shale: Study guide and reference source: New York, Springer-Verlag, 303 p.

Reading, H.G. & Richards, M., 1994, Turbidite systems in deep-water basin margins classified by grain size and feeder system: AAPG Bulletin, v. 78, p. 792-822.

Rebesco, M., Hernandez-Molina, F.J., van Rooij, D. & Wahlin, A., 2014, Countourites and associated sediments controlled by deep-water circulation processes: State-of-the-art and future considerations: Marine Geology, v. 352, p. 111-154.

Ruppel, S.C. & Ward, W.B., 2013, Outcrop-based characterization of the Leonardian carbonate platform in west Texas: Implications for sequence-stratigraphic styles in the Lower Permian: AAPG bulletin, v. 97, no. 2, p. 223-250.

Ruppel, S.C., Ward, W.B., Ariza, E., & Jennings, Jr., J.W., 2000, Cycle and sequence stratigraphy of Clear Fork reservoir equivalent outcrops: Victorio Peak Formation, Sierra Diablo, Texas, in Lindsay, R.F., Trentham, R.C., Ward, R.F. & Smith, A.H. eds., Classic Permian geology of west Texas and southeastern New Mexico: 75 years of Permian Basin oil and gas exploration and development: Geo 2000 field trip guidebook, West Texas Geological Society, v. 00-108, p. 109-128.

Rygel, M.C., Fielding, C.,R., Frank, T.D. & Birgenheier, L.P., 2008, The magnitude of Late Paleozoic glacioeustatic fluctuations: a synthesis: Journal of Sedimentary Research, v. 78, p. 500–511.

Schieber, J., Southard, J. & Thaisen, K., 2007, Accretion of mudstone beds from migrating floccule ripples: Science, v. 318, no. 5857, 1760-1763.

Schieber, J. & Southard, J.B., 2009, Bedload transport of mud by floccule ripples—Direct observation of ripple migration processes and their implications: Geology, v. 37, no. 6, p. 483-486.

Scholle, P.A. & Ulmer-Scholle, D.A., 2003, A color guide to the petrography of carbonate rocks: grains, textures, porosity, diagenesis: AAPG Memoir 77, 474 p.

Selley, R., 2000, Applied sedimentology: Academic Press, San Diego, 523 p.

Sen Gupta, B.K. & Machain-Castillo, M.L., 1993, Benthic foraminifera in oxygen-poor habitats, in Langer, M.R., ed., Foraminiferal microhabitats: Marine Micropaleontology, v. 20, p. 183-201.

Shanmugam, G., 2006, Deep-water processes and facies models: Implications for sandstone petroleum reservoirs: Amsterdam, Elsevier, Handbook of petroleum exploration and production, v. 5, 476 p.

Shanmugam, G., 2012, New perspectives on deep-water sandstones: Origin, recognition, initiation, and reservoir quality: Amsterdam, Elsevier, Handbook of petroleum exploration and production, v. 9, 524 p.

Silver, B.A. & Todd, R.G., 1969, Permian cyclic strata, northern Midland and Delaware Basins, West Texas and southeastern New Mexico: AAPG Bulletin, v. 53, p. 2223–2251.

Sivils, D., 2001, Examples of Wolfcampian debris flow deposits from the Eastern Shelf of the Midland Basin, Glasscock County, Texas, in Stoudt, E.L. & Sivils, D.J., eds., Wolfcampian of West Texas (Permian Basin, Sierra Diablo and Hueco Mountains) shelfal and periplatform carbonate reservoirs and outcrop analogs: Core workshop and field trip guidebook, Permian Basin Section, SEPM Publication 2001-41, p. 4-1-4-2.

Sloss, L.L., 1988, Tectonic evolution of the craton in Phanerozoic time, in Sloss, L.L., ed. Sedimentary cover – North American Craton, U.S.: The Geology of North America, Geological Society of America, v. D-2, p. 25-51.

Spain, D.R. & Anderson, G.A., 2010, Controls on reservoir quality and productivity in the Haynesville Shale, northwestern Gulf of Mexico Basin: Gulf Coast Association of Geological Societies, Transactions, v. 60, p. 657-668.

Stowe, D.A.V. & Tabrez, A.R., 1998, Hemipelagites: processes, facies and model, in Stoker, M.S., Evans, D. & Cramp, A., eds., Geological processes on continental margins: Geological Society of London, Special Publication 129, p. 317-337.

Stowe, D.A., Howell, D.G. & Nelson, C.H., 1985, Sedimentary, tectonic, and sea-level controls, in Bouma, A.H., Normark, W.R. & Barnes, N.E., eds., Submarine fans and related turbidite systems: New York, Springer-Verlag, p. 15-23.

Talling, P.J., Masson, D.G., Sumner, E.J. & Malgesini, G., 2012, Subaqueous sediment density flows: Depositional processes and deposit types: Sedimentology, v. 59, no. 7, p. 1937-2003.

Tyler, N., Ghoston, J.C. & Guevara, E.H., 1997, Basin morphological controls on submarine-fan depositional trends: Spraberry Sandstone, Permian Basin, Texas: Geological Circular, University of Texas at Austin, Bureau of Economic Geology, 43 p.

Udden, J.A., 1917, Notes on the geology of the Glass Mountains: University of Texas Bulletin, no. 1753, p. 1-59.

Veevers, J.J. & Powell, M., 1987, Late Paleozoic glacial episodes in Gondwanaland reflected in transgressive-regressive depositional sequences in Euramerica: Geological Society of America Bulletin, v. 98, p. 475-487.

Sageman, B.B., Murphy, A.E., Werne, J.P., Ver Straeten, C.A, Hollander, D.J. & Lyons, T.W., 2003, A tale of shales: the relative roles of production, decomposition, and dilution in the accumulation of organic-rich strata, Middle-Upper Devonian, Appalachian basin: Chemical Geology, v. 195, p. 229-273.

Wahlman, G.P. & Tasker, D.R., 2013, Lower Permian (Wolfcampian) carbonate shelf-margin and slope facies, Central Basin Platform and Hueco Mountains, Permian Basin, West Texas, USA, in Verwer, K., Playton, T.E., and Harris, P.M., eds., Deposits, architecture and controls of carbonate margin, slope and basinal settings: SEPM Special Publication No. 13, p. 305–333.

Walker, R.G., 1965, The origin and significance of the internal sedimentary structure of turbidites: Proceedings of the Yorkshire Geological Society, v. 35, p. 1-32.

Walker, D.A., Golonka, J., Reid, A.M. & Reid, S.A.T., 1991, The effects of late Paleozoic paleolatitude and paleogeography in the Midland basin, Texas, in Candelaria, M.P., ed., Permian basin plays – tomorrow's technology today: West Texas Geological Society Publication no. 91-89, p. 141-162.

Wetzel, A., 1984, Bioturbation in deep-sea fine-grained sediments, influence of sediment texture, turbidite fequency and rates of environmental change, in Stowe, D.A.V. & Piper, D.J.W., eds., Fine-grained sediments: Deep-water processes and facies: Geological Society of London, Special Publicaton no. 15, p. 595-608.

Wignall, P.B., Bond, D.P.G., Kuwahara, K., Kakuwa, Y., Newton, R.J. & Poulton, S.W., 2010, An 80 million year oceanic redox history from Permian to Jurassic pelagic sediments of the Mino-Tamba terrane, SW Japan, and the origin of four mass extinctions: Global and Planetary Change, v. 71, p. 109-123.

Wilson, J.L., 1975, Carbonate facies in geological history: New York, Springer-Verlag, 471 p.

Yang, K. & Dorobek, S.L., 1995, The Permian Basin of west Texas and New Mexico: Tectonic history of a “composite” foreland basin and its effects on stratigraphic development, in Dorobek, S. L. & Ross, G. M., eds., Stratigraphic evolution of foreland basins: SEPM Special Publication 52, p. 149-174.

APPENDIX

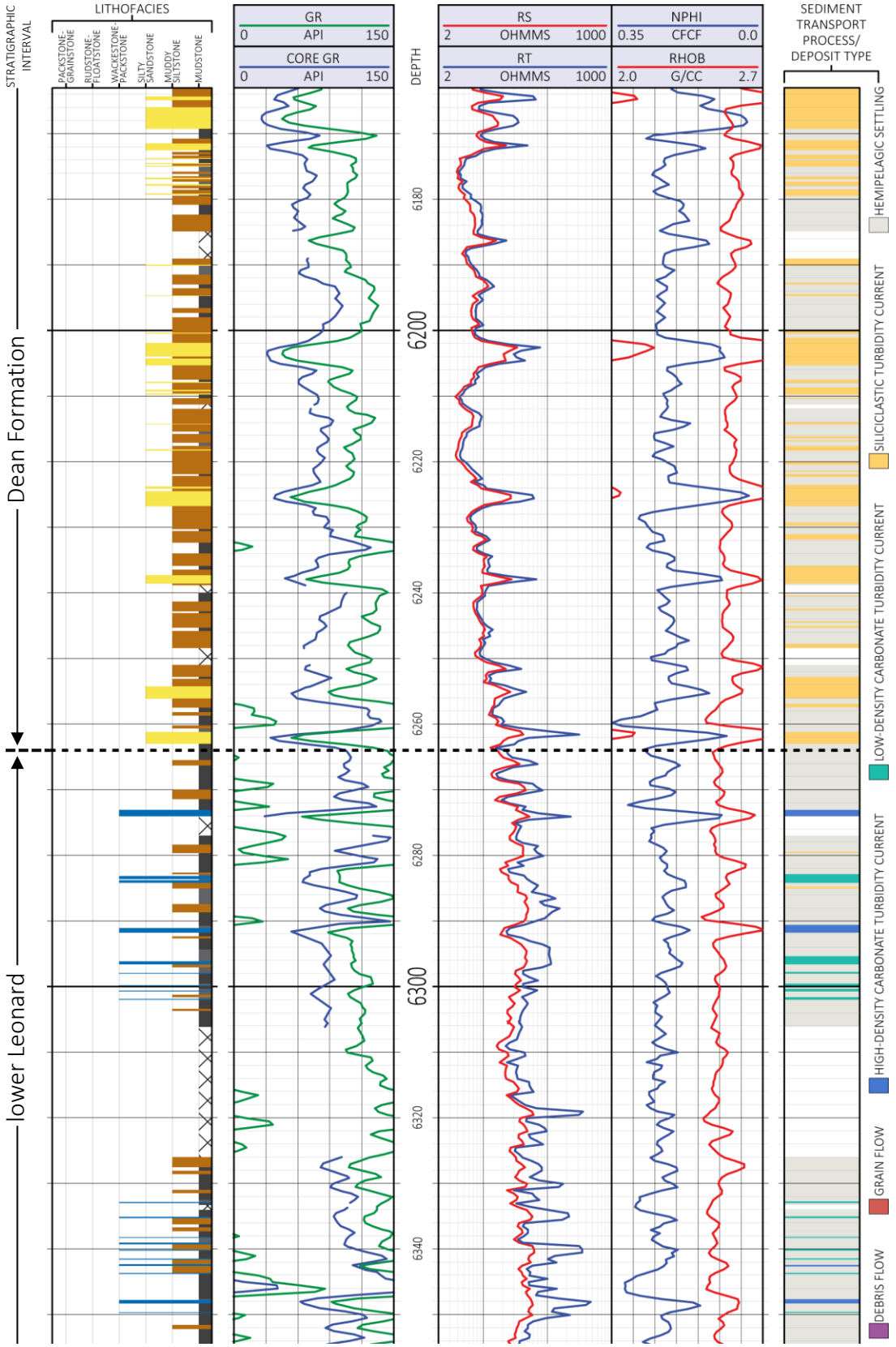

Figure A1. Stratigraphic column of the Mayer 4901 well including lithofacies, interpreted sediment transport processes, and wireline log data.

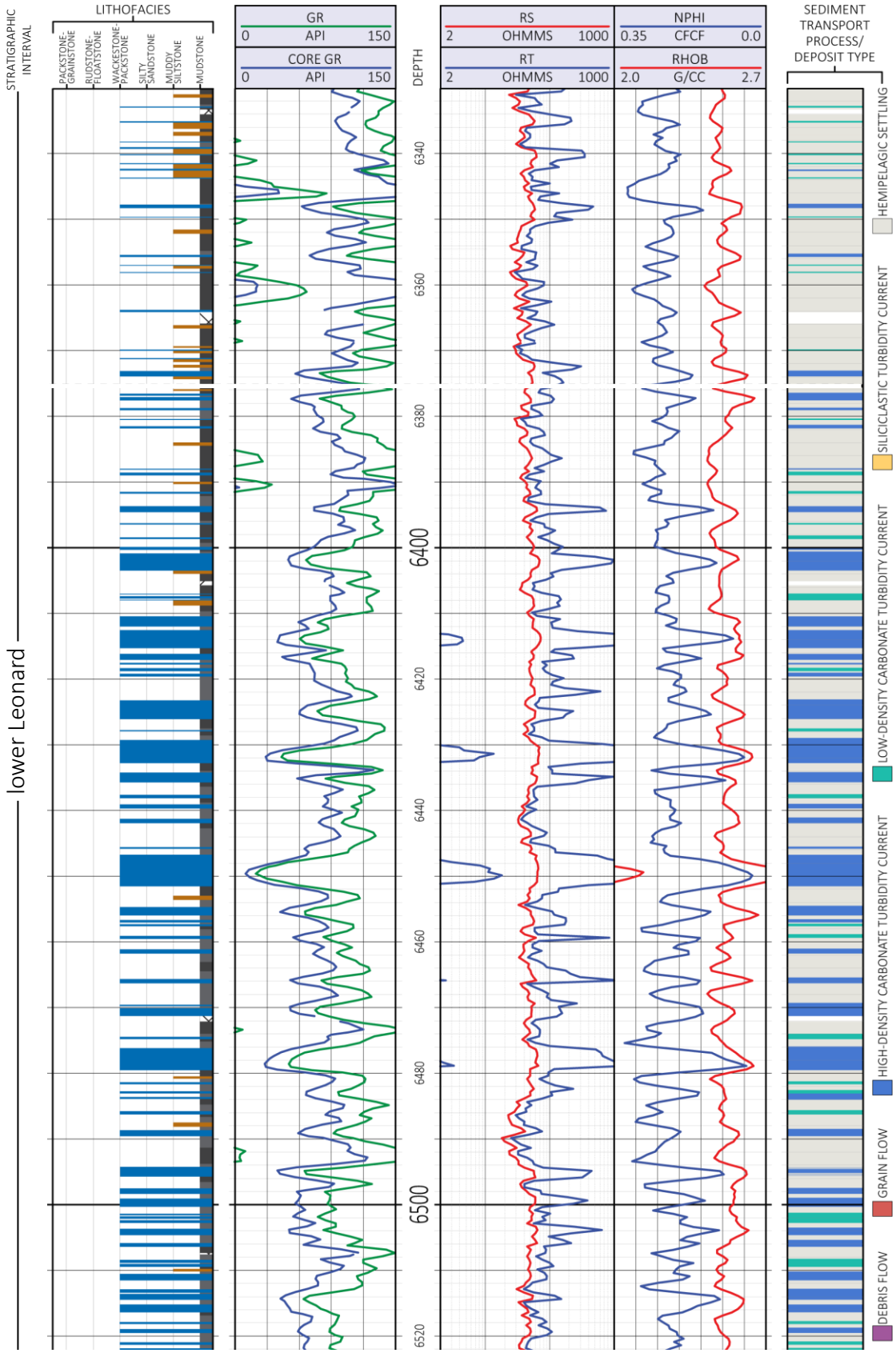

Figure A2. Stratigraphic column continued.

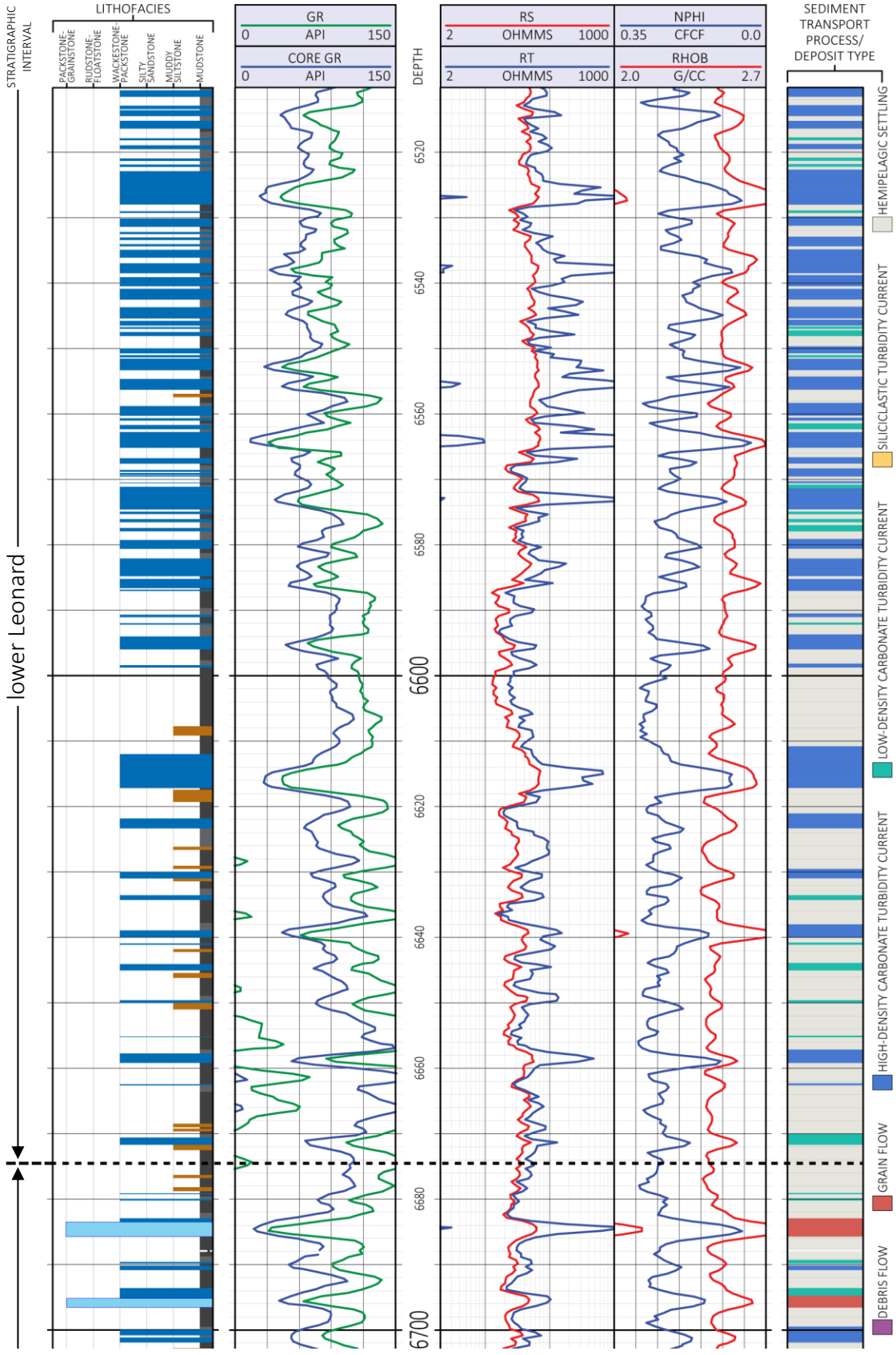

Figure A3. Stratigraphic column continued.

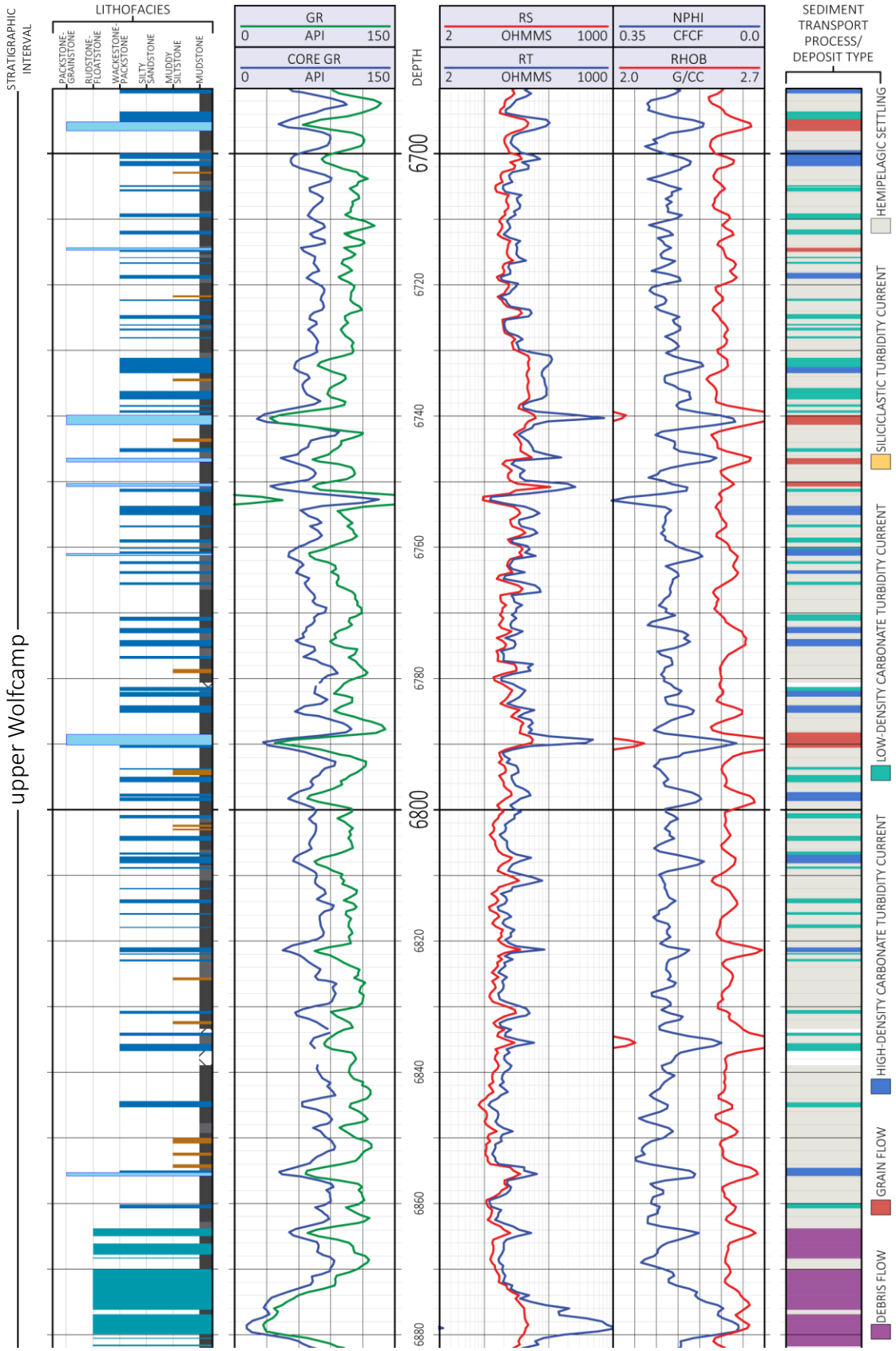

Figure A4. Stratigraphic column continued.

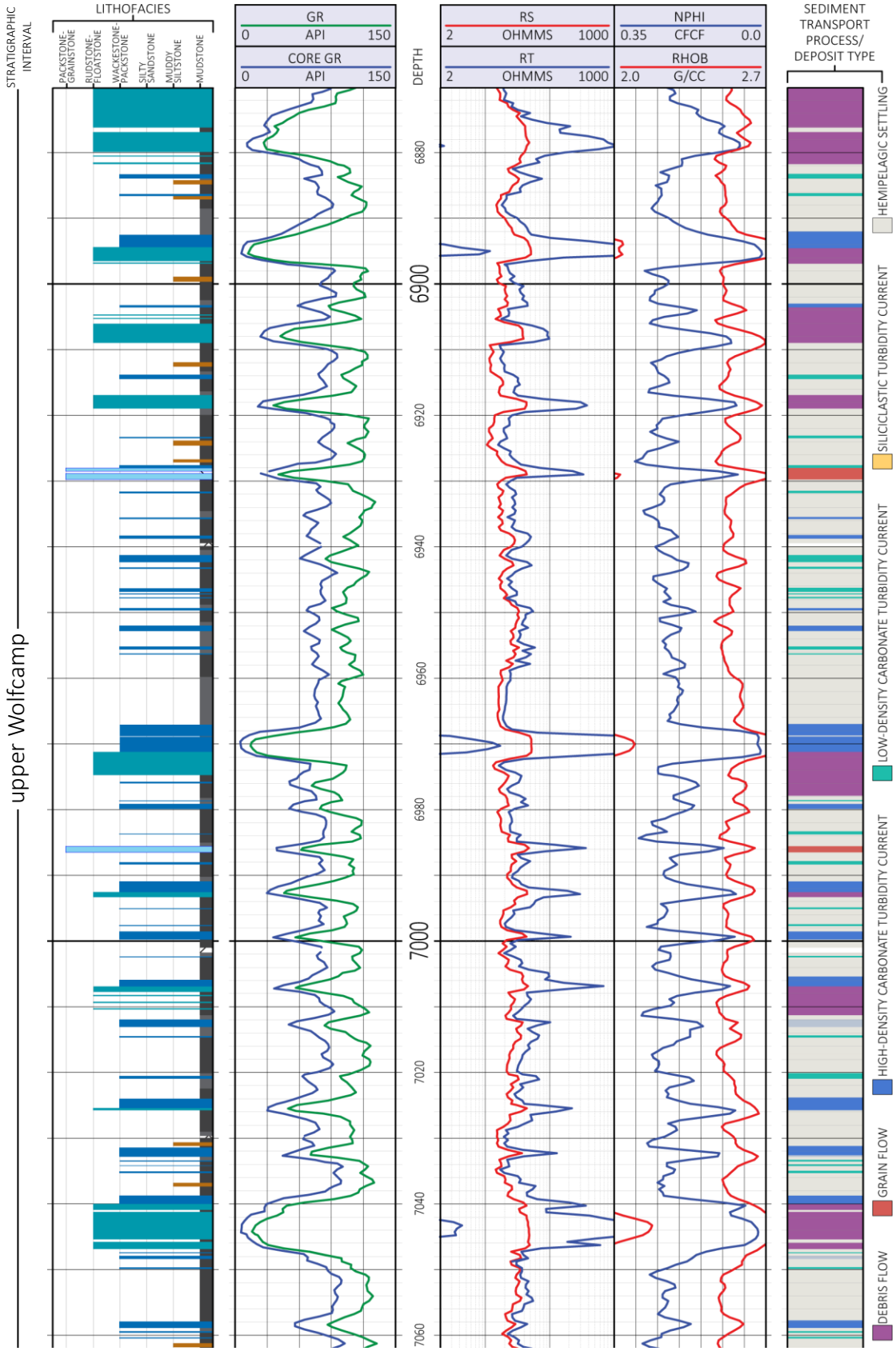

Figure A5. Stratigraphic column continued.

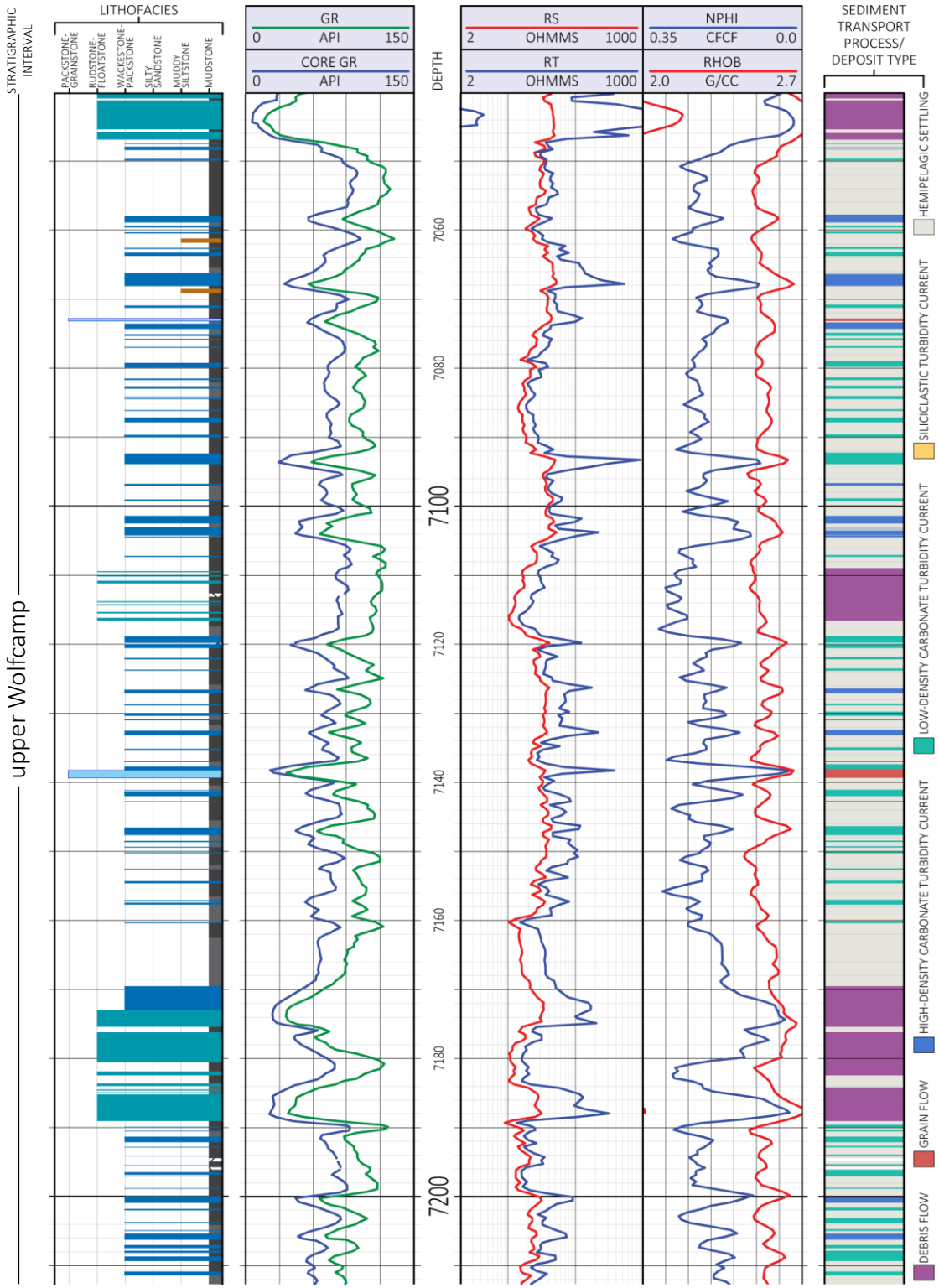

Figure A6. Stratigraphic column continued.

VITA

Zakory Dean Ward

Candidate for the Degree of

Master of Science

Thesis: DEPOSITIONAL PROCESSES AND ENVIRONMENTS IN WOLFCAMPIAN-LEONARDIAN STRATA, SOUTHERN MIDLAND BASIN, TEXAS

Major Field: Geology

Biographical:

Education:

Completed the requirements for the Master of Science in Geology at Oklahoma State University, Stillwater, Oklahoma in May, 2017.

Completed the requirements for the Bachelor of Science in Geology at Iowa State University, Ames, Iowa in 2013.

Experience:

Internship at Cantrell Energy Corporation in Ada, OK (2014).

Internship at EOG Resources in Corpus Christi, TX (2015).

Internship at WPX Energy in Tulsa, OK (2016).

Geoscientist I at WPX Energy in Tulsa, OK (2016-present)

Professional Memberships:

AAPG, GSA, SEG, SPE, TGS, and OCGS